Basin scale distribution of organic matter in marine fine-grained sedimentary rocks: Insight from sequence stratigraphy and multi-proxies analysis in the Montney and Doig formations

Vincent Crombez, François Baudin, Sébastien Rohais, Laurent Riquier, Tristan Euzen, Stanislas Pauthier, Mathieu Ducros, Benoît Caron, Noga Vaisblat

Basin scale distribution of organic matter in marine fine-grained sedimentary rocks: insight from sequence stratigraphy and multi-proxies analysis in the Montney and Doig Formations

CROMBEZ Vincent*[1 2], BAUDIN François [2], ROHAIS Sébastien [1], RIQUIER Laurent [2], EUZEN Tristan [3], PAUTHIER Stanislas[2 1], Mathieu DUCROS [1], CARON Benoit[2], VAISBLAT Noga[4].

1 - IFP Energies nouvelles, 1 et 4 Avenue de Bois-Préau, 92500, Rueil-Malmaison, France.

2 - Sorbonne Universités, UPMC Univ. Paris 06, CNRS, ISTeP, 75005, Paris, France.

3 - IFP Technologies (Canada) Inc., Suite 810, 744 - 4th Avenue S.W., Calgary, Alberta, Canada.

4 - Department of Earth and Atmospheric Sciences, University of Alberta, 1-26 ESB, Edmonton, Alberta, Canada.

* Corresponding author e-mail: crombez.v@gmail.com

Revised manuscript submited to: Marine and Petroleum Geology

The 15/09/2015

ABSTRACT

The occurrence of hydrocarbons in self-sourced reservoirs strongly depends on the concentration and maturity of organic matter in sediments. Therefore, understanding the distribution of organic heterogeneity at the time of deposition is key to reduce the risk in exploration and development of unconventional resources. This study focuses on the Lower and Middle Triassic Montney and Doig Formations (Alberta and British Columbia). Samples from outcrops, cores and cuttings were analyzed for organic content with a Rock-Eval VI and for major and trace element concentration using ICP-MS and ICP-AES techniques. The interpretation of the analysis results in relation with the stratigraphic architecture provides a mean to better understand the distribution of the organic heterogeneities and the variations of primary productivity, sedimentation rates and anoxia that control the development of source rocks.

The key findings of this analysis are:

- The basin-scale distribution of the organic matter suggests that the two major source-rock intervals of the Lower and Middle Triassic correspond to the sequence 3 (Spathian Montney unit) and to the transgressive systems tract of sequence 4 (Doig phosphate zone).
- The dominant controls on organic matter accumulations vary through time. The Montney source-rock interval is interpreted to be associated with a major basin restriction triggering anoxia during a second-order falling stage of relative sea level. The organic accumulation of the Doig phosphate zone is interpreted as being controlled by a sharp decrease of the sedimentation rate, combined with an increase of the primary productivity.
- The spatial and temporal variations of anoxia, primary productivity and dilution reflect the geodynamic evolution of the basin that ultimately controls the basin physiography as well as the sources of nutrient and sediments.

HIGHLIGHTS

The Montney and Doig Formations mainly present amorphous organic matter.

Rock-Eval data integration in stratigraphic framework shows two organic rich layers.

Ni and Cu variations suggest an increased primary productivity in the Doig Phosphate.

Redox proxies suggest anoxic intervals in the Upper Montney and the Doig Phosphate.

KEYWORDS

Petroleum source rocks; Triassic; Montney and Doig Formations; Organic matter; Primary productivity; Redox conditions; Sedimentation rates; Canada.

1. INTRODUCTION

With the development of self-sourced and closely associated tight reservoirs, there is a need for a better understanding of the origin and distribution of primary organic matter (OM) in source rocks (Schwarzkopf, 1993; Tommeras and Mann, 2008; Ducros *et al.,* in press). Stratigraphic framework characterization is the first and main step needed to quantify and discuss the processes controlling the distribution of OM (Creaney and Passey, 1993; Myers, 1996; Huc *et al.,* 2005; Van Buchem *et al.,* 2005; Slatt and Rodriguez, 2012). Such integrated workflow gathering information on organic productivity, preservation and dilution at basin scale remains a challenge especially as geodynamic and climatic setting induce a large diversity of organic-rich deposits (Huc *et al.,* 2005).

Our work focuses on one of the largest unconventional play of Canada: the Montney and Doig Formations of the Lower and Middle Triassic interval (~ 252 - 235 Ma) of Western Canada. The amount of data available due to an extensive oil and gas exploration in the area and the presence of time equivalent outcrops in the fold and thrust belt of the Canadian Cordillera, makes this interval an attractive case study to analyze OM distribution in sedimentary basins. This study is built on a database including core, cutting and outcrop descriptions and samples as well as wireline logs. Geochemical and organic petrographical analyses (palynofacies, Rock-Eval, Major and Trace Metal Elements) were then performed on selected samples. Finally, the results were integrated in a

sequence stratigraphic framework in order to discuss the main factors controlling the distribution of OM in the studied interval.

2. THE MONTNEY AND DOIG FORMATIONS

2.1. Generalities

The Montney, Doig and Halfway Formations are preserved in the foreland basin of the Canadian Cordillera and in time equivalent outcrops in its fold and thrust belt (**figure 1**). These Lower and Middle Triassic Formations have been studied since the 60's (Armitage 1962). The Montney and Doig Formations are mostly composed of fine-grained dolomitic sandstone and siltstone with subordinate amount of shale and moderate clay content (Davies, 1997a; Zonneveld *et al.,* 2010; Chalmers and Bustin, 2012; Euzen *et al.,* 2015). They were deposited on the western margin of Pangea (Davies *et al.,* 1997). This location is considered as a passive margin during the Devonian and a foreland basin during the Jurassic. Doubts remain on the precise paleogeographic settings: foreland basin (Golding *et al.,* 2015a) versus passive margin during the time of the deposition of the studied interval (Monger and Price, 2002).

2.2. Stratigraphic settings and chronostratigraphy

The stratigraphic framework used in this paper is based on a recent regional sequence stratigraphic interpretation of the Lower and the Middle Triassic in the Western Canada Sedimentary Basin (e.g. Crombez, 2016). Based on more than 400 wells, it shows that the studied interval can be subdivided into two second-order sequences A and B and that sequence A can be further subdivided into three third order sequences 1, 2 and 3. Within sequence A, the maximum backstepping of the sedimentary system occurs during the second sequence (**figure 2**). Based on the biostratigraphic works of Orchard and Zonneveld (2009) and Golding *et al.* (2015b), sequence A and B are respectively Lower Triassic and Middle Triassic in age. Within sequence A, sequence 2 was deposited above the Induan-Olenekian boundary and sequence 3 lays on top of the Smithian-Spatian boundary. According to biostratigraphic data, the top of sequence B is older than the Ladinian-Carnian boundary (Orchard

and Zonneveld, 2009). Integrating these recent developments (Crombez, 2016) in Davies et al., 1997 stratigraphic framework, the Montney Formation corresponds to sequence A. In this first second order sequence, sequence 1 can be considered as the Lower Montney, the sequence 2 as the Middle Montney and sequence 3 as the upper Montney whereas the Doig and Halfway Formations are part of sequence B. As the Montney Formation is interpreted as a second order cycle, the sequence 1 and the transgressive system tract (TST) 2 therefore represents a second order TST, the sequence 2 a second order HST and the sequence 3 a second order FSST (Crombez, 2016). From this work, as sequence B records the expression of a second order cycle, TST4 and HST4 can be considered as second order system tracts or third order sequences.

The **figure 2** illustrates the position of the studied well and outcrop (restored location) sections within the stratigraphic framework of the basin. A recent study suggests that the Montney and Doig Formations were deposited in a fore-arc basin connected with the open marine setting to the Northwest (Rohais *et al.,* 2016). The stratigraphic architecture of sequence A suggests a basin with a WNW-ESE axis and sedimentary inputs coming from East and Southeast. The distribution of thickness and facies in sequence B suggests a NW-SE basin axis with an additional sedimentary source to the West (**Error! Reference source not found.**). This change in sediment source areas and the clockwise rotation of the basin axis are interpreted to be linked to the evolution of the proto-Canadian Cordillera (Crombez, 2016; Rohais *et al.,* 2016).

3. DATA AND METHODS

3.1. Data

For this study, data were collected from both outcrop in the Canadian Cordillera and subsurface in the foreland basin (**figure 1**). In Alberta, the cuttings from the Montney-Doig-Halfway intervals were sampled in 7 wells and in addition, 14 cores were also sampled. In British Columbia, the cuttings of the studied interval were sampled in 3 wells. Moreover, 4 cores including a 300m long core and one outcrop (Brown Hill, BH on **figure 1**) were sampled. In total, 365 samples collected from cores, 498

from cuttings and 176 from outcrops were available for this work. The results of the present study is illustrated along a SE-NW section composed of 7 wells with cuttings sampled each 5-10m and a 300m long core, sampled each 5-10m, with additional constraints from both outcrops and subsurface (**figure 1**).

3.2. Methods

The workflow developed for this study unfolds as follow: (1) The characterization of the organic content in the studied interval, using Rock-Eval analyses (Espitalie *et al.,* 1986; Behar *et al.,* 2001) and palynofacies study (Tyson, 1995). (2) The study of the distribution of the organic rich layers in the stratigraphic framework. (3) The study of paleoenvironmental conditions through variations of major and trace element concentrations and mineralogy in order to highlight the dynamic of the primary productivity, the dilution by non-organic element and the O_2 levels along four sections (Brumsack, 2006; Tribovillard *et al.,* 2006; Algeo and Tribovillard, 2009 and references herein).

3.2.1. Rock-Eval pyrolysis and hydrocarbons extraction

Routine source rock analyses were carried out on 900 samples with a Rock-Eval VI. The bulk-rock basic cycle, used for these routine analyses, is described by Behar *et al.* (2001). 50 to 70 mg of powdered sample is heated in an open pyrolysis system under non-isothermal condition (from 300 °C to 650 °C). During this pyrolysis, the amount of hydrocarbons released is measured by a flame ionization detector (FID) and CO and CO_2 release are monitored with an infrared (IR) detector. The residual sample is then put in an oxidation oven where it is heated (from 300 °C to 800 °C) under artificial air (N_2/O_2: 80/20). During this combustion, the amount of CO and CO_2 released are monitored with an IR detector.

In addition to the bulk-rock samples, organic solvent extraction was performed on selected samples. The powdered sample was placed in a solution of dichloromethane and methanol (1/1) in an ultrasonic bath for 30 min. The sample was then filtered and placed in a drying oven for 30 min. Finally the sample was analyzed with the basic Rock-Eval method described above.

3.2.2. Palynofacies

In addition to the source rock evaluation, palynofacies analyses were carried out on 26 selected samples. The preparation of the samples consists in the dissolution of 2 g of crushed rock in successive acid bath. The sample was placed in a cold solution of hydrochloric acid (70 %) for 180 min. After multiple rinsing, the residual sample was placed in a cold solution of hydrofluoric acid (70 %) for 180 min. Again, after multiple rinsing, the residual sample is place in a hot (40 °C) solution of hydrochloric acid (70 %) for 180 min. Finally, after multiple rinsing, the residual sample was sieved with a 15µm filter and the filtrate was mounted between two glass slides.

The slides were then observed with an optical microscope under different magnifications in order to classify the organic particles in three categories following the classification of Tyson (1995): the amorphous organic matter (AOM), the phytoclasts and the palynomorphs.

3.2.3. Initial TOC computation

In order to better understand the distribution of organic matter at the time of deposition (before thermal maturation), Rock-Eval analysis and palynofacies were used to estimate the initial total organic carbon (TOC_{ini}). The equation (**Equation** Error! Reference source not found.**1**) used for the computation of the TOC_{ini} is based on carbon mass balance and is similar to the formula proposed by Jarvie (2012).

$$TOC_{ini} = \frac{TOC-(S1+S2)\times 0.083}{1-(HI_{ini}/1200)} \qquad \textbf{(Equation 1)}$$

This equation uses the total organic carbon (TOC), the free hydrocarbons (S1) and the oil potential (S2) from Rock-Eval analysis, and requires an estimation of the initial hydrogen index (HI_{ini}). The HI_{ini} was estimated using the palynofacies analyses that provide insight into the nature and quality of the OM. The values of HI_{ini} used in this study are 700 mgHC/gTOC for type I organic matter, 450 mgHC/gTOC for type II and 125 mgHC/gTOC for type III (Espitalié *et al.,* 1986; Jarvie *et al.,* 2007).

3.2.4. Inductively Coupled Plasma Mass Spectrometry (ICP-MS) and Inductively Coupled Plasma Atomic Emission Spectrometry (ICP-AES)

Elementary analyses of samples from wells 0/14-14-76-12W6 and 0/06-33-72-25W5 and from Brown Hill outcrop were performed with an ICP-MS for trace elements and an ICP-AES for major elements. Samples were powdered with an agate mortar beforehand. Then, 50 mg of sample was solubilized using a solution of hydrochloric acid (70 %) and a solution of boric acid (45 %). In order to dissolve entirely the OM, 2 ml of a hydrogen peroxide solution were added to the samples with a high TOC. The residual samples were then diluted 10,000 times for the ICP-MS analyses and 1,000 for the ICP-AES analyses. International (ATHO-G from Borisova *et al.,* 2010; AGV-1, BCR-2, BH-VO2 and BIR-1 from the USGS) and in house standards were used and several duplicates were analyzed in order to control the accuracy of the measurements. A total of 244 samples were analyzed with this method. Elementary analyses from well 0/16-17-83-25W6 were performed by ACT Labs following their 4A-4B protocols. A total of 138 samples were analyzed with this method. In the present work element concentration (ppm or %) refers to weigh ratios.

In order to investigate the vertical and the lateral variations of metal trace elements (MTE), the concentration of MTE was divided by the Aluminum content of the sample and normalized to the upper continental crusts (UCC) by computing an enrichment factors (EF) (Taylor and McLennan, 1985; McLennan, 2001):

$$EF_E = \frac{\frac{[E]}{[Al]}sample}{\frac{[E]}{[Al]}UCC} \quad \textbf{(Equation 2)}$$

With EF_E the enrichment factor of E; [E] the atomic concentration of E (ppm) and [Al] the concentration of aluminum (ppm).

3.2.5. Mineralogical analyses

In addition to core and outcrop descriptions, cuttings from one well were sampled in order to quantify the mineralogy of the Triassic strata. QEMSCAN analyses (Gottlieb *et al.,* 2000) were performed by SGS Canada Inc. on 72 samples. QEMSCAN automated mineralogical analysis is based on backscattered-electron imaging and energy dispersive X-ray spectroscopy techniques.

3.2.6. Weathering index of Parker (WIP) and chemical index of alteration (CIA)

Based on elemental major element concentrations, the weathering index of parker (WIP, Parker, 1970) and the chemical index of alteration (CIA, Nesbitt and Young, 1982) provide information on the maturity of siliciclastic sediments:

$$WIP = \left(\frac{[Na]^*}{0.35} + \frac{[Mg]^*}{0.9} + \frac{[K]^*}{0.25} + \frac{[Ca]^*}{0.7}\right) \times 100 \quad \textbf{(Equation 3)}$$

$$CIA = \left(\frac{[Al_2O_3]}{[Al_2O_3]+[Na_2O]+[K_2O]+[CaO]}\right) \quad \textbf{(Equation 4)}$$

Where [E] is the atomic concentration of E (ppm) and [E]* represent the atomic concentration of an element divided by its atomic weight. In order to reflect chemical variations associated with climatic changes and the weathering of siliciclastic minerals, the [Ca] and [CaO] values used in the **equation 3 and 4** were corrected for each samples to remove the effect of carbonate minerals using QEMSCAN analysis. WIP and CIA indexes were only calculated on one well where both elemental analysis and QEMSCAN data were available on the same samples (0/14-14-76-12W6). Furthermore, the sodium (Na) concentration was not measured on this well, but the impact of Na on these indexes is likely negligible based on its low concentration in other wells of this study (average of 0.8% in well 0/16-17-83-25W6).

4. RESULTS

4.1. Characterization of the organic content

4.1.1. Rock-Eval analyses

Most of the studied samples have Rock Eval TOC values ranging between 0.25 and 1.75 wt%, with a mean TOC of 1.28 wt% (see **figure** 7). However locally, organic-rich intervals present TOC higher than 4 wt% in the Montney Fm. and can reach up to 13 wt% in the Doig phosphate zone (TST4). The wide range of Tmax (from 397 to 479 °C) of our dataset is globally consistent with published vitrinite reflectance data (Rokosh *et al.* 2012; Romero *et al.,* 2016) and suggests NE-SW increasing maturity trend from immature to overmature. The wide range of maturity may induce an under or over estimation of the *in-situ* TOC. Indeed, the dysmigration of the generated HC will lead to the underestimation of the TOC whereas the contamination by migrated HC will lead to the overestimation of the TOC. Rock-Eval pyrolysis results of the low maturity samples show that most of the HI values fall between 150 and 450 mgHC/gC. This observation suggests that the OM found in the Montney and Doig Formations is mainly of Type II and Type III (**figure 3**).

Detailed analysis of Rock-Eval pyrograms shows that the S2 peak often presents a shoulder during the beginning of the temperature increasing (between 300 °C and 450 °C, **figure 4**). This shoulder can be interpreted in two different ways: there are two types of kerogen in the sample, or there is a presence of heavy hydrocarbons (Grundman *et al.,* 2012). **Figure 4** presents the pyrogram of both bulk-rock (BR) and extracted bulk-rock (eBR) samples. The analysis of both bulk-rock and extracted sample shows that the S2 is composed of both soluble and non-soluble OM, likely representing respectively heavy hydrocarbons and primary kerogen (**figure 4**). According to the work of Behar *et al.* (2008) and considering the low maturity of this sample (Tmax = 439 °C), those heavy hydrocarbons may come from the early cracking of the kerogen.

4.1.2. Palynofacies studies

The investigated samples contain mainly AOM (**figure 5**). In the analyzed samples, only a small proportion of the OM derives from woody and terrestrial debris, regardless of the sedimentary facies (SP and PM on **figure 5 B, C and I**). The absence of damaged terrestrial OM showing a transformation

from undamaged particles to AOM suggests that the AOM was more likely derived from marine rather than terrestrial sources (Tyson, 1995).

4.2. Distribution of the organic content in the stratigraphic framework

4.2.1. TOC and TOC_{ini} in the stratigraphic framework

The Rock-Eval results show that the two samples with the lowest maturity present high to moderate HI (respectively 549 and 373 mgHc/gTOC). This is consistent with of a good Type II marine kerogen and a fair Type II/III kerogen. The palynofacies analyses paired with the Rock-Eval measurements suggest that regardless of the sedimentary facies, the AOM mainly derives from marine sources, typically having an initial HI (HI_{ini}) between 350 and 600 mgHC/gTOC. These two values were used to compute a maximum and a minimum value of TOC_{ini}. In low maturity areas (Tmax < 450°C), the computed TOC_{ini} values likely reflect the initial organic content of the sediment. On the other hand, in more mature areas (Tmax > 450°C), TOC_{ini} computation can be affected by the secondary cracking of migrated oil. **Figure 6 and 7** illustrate that sequence 3 and TST4 are the two main organic-rich intervals of this succession based on TOC_{ini} computation. In low maturity areas TOC_{ini} is close to present day TOC, whereas in more mature areas, TOC_{ini} can be up to twice as high as present day TOC (with HI_{ini} = 600).

The vertical distribution of TOC values within the stratigraphic framework highlight major differences between sequences (**figure** 6 and 7). Sequences 1 and 2 have low background present day TOC (respectively 1.3 and 0.9 wt% on average), with localized organic-rich intervals up to about 3 wt% (**figure 7**). Sequence 3 has higher background TOC (average of 2.2 wt%) and fewer low TOC values (<1 wt%) than sequence 1 and 2. TOC_{ini} values can reach up to 9 wt% in LST3. The base of Sequence 4 is the richest interval in OM, with TOC_{ini} up to 14% (TST4=phosphate zone), but the rest of sequence 4 is organic-lean (average of 1.1wt%). The two main organic-rich intervals LST3 and TST4 show contrasting spatial distributions of the OM:

In LST3, the organic content increase in the deeper central part of the basin at that time (offshore environment).

In TST4, TOC increase towards both margins of the basin (well 0/16-17-83-25W6 and 07-14-74-06W6 on **figure 6**) while lower values are observed toward the axis of the basin (well 0/14-14-76-12W6 on **figure 6**).

4.2.2. Sedimentology of organic rich intervals

In this section, we illustrate the sedimentological features of the organic-rich intervals of sequence 3 and 4. **Figure 8** presents a synthetic sedimentary section from the sequence boundary 3 (SB3) up the maximum flooding surface 4 (MFS4). This interval dominantly consists of wave-dominated deposits, from offshore (bathymetry ≈ 200 m) to shoreface depositional environments (**figure 8**, Crombez, 2016). In both sequences, organic-rich intervals correspond to offshore depositional environments. Sequence 3 presents a thick continuous interval of prograding deposits from offshore to lower shoreface (e.g. from 2380 to 2260 m on **figure 8**) whereas TST4 consists of thinly interbedded offshore and offshore transition deposits (e.g. from 2255 to 2240 m on **figure 8**). In sequence 3, the high TOC intervals are associated with pyrite and phosphate grains, but with only rare bioturbations (from 2380 to 2320 m on **figure 8**). In contrast, organic-rich layers in TST4 are associated with erosive lags, shell debris as well as pyrite and phosphate grains whereas bioturbations are present in the coarse-grained interbedded shallower deposits (from 2255 to 2240 m on **figure 8**). These differences suggest that the organic rich offshore deposits of TST4 are shallower than the offshore deposits of sequence 3

4.2.3. Vertical and lateral variation of the sediment rates

Sequence stratigraphic surfaces provide time lines across the basin (Crombez, 2016) and allowed for the computation of average sedimentation rates (SR) in the studied intervals. The sequence A was deposited during the lower Triassic (approximately 5 My) and the sequence B during the Middle Triassic (approximately 8 My).

The **figure 9** presents a cross-plot of the distribution of TOC_{ini} versus the SR in the third order sequences along 8 sections. It shows that sequence B presents lower sedimentation rates (SR < 6 cm/ka) than sequence A (SR < 16 cm/ka). More precisely it shows that sequences 1 to 3 present increasing average sedimentation rates (average SR from 4 cm/ka to 12 cm/ka) whereas HST4 present lower sedimentation rates than TST4 (respectively average SR: 2 cm/ka and 3 cm/ka). On **figure 9**, the sequences 1 and 2 present decreasing TOC_{ini} concentration (from 3 to 0.2 wt%) with increasing SR (from 16 to 4 cm/ka). The sequence 3 presents a similar evolution but with a steepest trend (TOC_{ini} from 7 to 3 wt% and SR from 12 to 16 cm/ka). The TST4 does not present a clear relation between TOC_{ini} accumulation and SR. On one side, the **figure 9** presents high TOC_{ini} (up to 15 wt%) associated with the highest SR of the TST4 (4 cm/ka) and on the other side it shows decreasing TOC_{ini} (from 2.5 to 0 wt%) with increasing SR (from 1 to 2 cm/ka). Lastly HST4 presents an increasing then decreasing TOC_{ini} (from 1 to 2.5 wt% then from 2.5 to 0 wt%) with increasing SR (from 0.3 to 4 cm/ka).

Tyson (2001) highlighted the impact of SR on OM accumulation. On one side, this study showed that, in oxic environments, a range of SR (from 2 to 20 cm/ka) is increasing OM preservation. In oxic intervals, the impact of the SR results in an increasing then decreasing TOC concentration with a maximum accumulation above 5 cm/ka. The cross-plots of sequences 1, 2 and of the HST4 highlight the direct impact of organic particles dilution: sequences 1 and 2 only present the decreasing TOC_{ini} whereas the HST4 presents both the increasing and decreasing trends linked to the ideal sedimentation rates interval. On the other side, in anoxic environments the preservation of the organic matter is assured and an increasing SR will only decrease the TOC (Tyson, 2001). The rapid increase of the TOC_{ini} in the Seq 3 and the complex relation between TOC_{ini} and SR in TST4 suggest that organic matter accumulation in TST4 and sequence 3 is not solely controlled by the dilution but by a complex combination of primary productivity, preservation and dilution.

4.3. Trace metal element variations

329 ***4.3.1. Copper (Cu) and Nickel (Ni) variations***

330 Organic productivity can be studied through several proxies, including Cu and Ni which are micro-
331 nutrients assimilated by the micro and macro-organisms (Calvert and Price, 1983; Calvert and
332 Pedersen, 1993; Whitfield, 2001; Brumsack, 2006; Tribovillard *et al.,* 2006; Schoepfer *et al.,* 2014). In
333 the present study, the vertical evolution of Ni/Al and Cu/Al are chosen to reflect the variations of
334 nutrients input in the basin which may be associated with primary organic productivity variations
335 (Whitfield, 2001; Brumsack, 2006; Tribovillard *et al.,* 2006)

336 The **figure 10** presents a cross-plot of the EF of Cu vs Ni at four different locations in the basin. In this
337 figure, most of EF of Cu and Ni are higher than 1. In comparison to black shale (Cretaceous and
338 present day, Brumsack, 2006) the EF of Cu and Ni remain low in the Montney and Doig Formations.
339 TST4 shows the highest EF in sections 0/16-17-83-25W6 section ($3 < EF(Ni) < 10$; $2 < EF(Cu) < 30$) and
340 0/14-14-76-12W6 ($EF(Ni) \approx 10$; $EF(Cu) \approx 2.5$). In these wells, samples with High TOC always have high
341 EF, however high EF does not automatically imply high TOC. No simple linear relation exists between
342 EF(Ni) or EF(Cu) and TOC.

343 The **figure 11** presents the vertical evolution of Cu/Al and Ni/Al along the four sections. In these
344 sections, Cu/Al ranges from 3.10^{-4} to more than 30.10^{-4} whereas Ni/Al ranges from 5.10^{-4} to 55.10^{-4}.

345 *0/16-17-83-25W6:*

346 In sequences 1 and 2, both ratios show little variations and stay low (Cu/Al ≈ 5.10-4 and Ni/Al ≈
347 7.5.10-4), slightly higher than the Upper crust average (Cu/Al = 3.1.10-4 and Ni/Al = 5.5.10-4).
348 Sequence 3 records a small increase in Cu/Al (from 5.10-4 to 6.10-4) and in Ni/Al (from 7.5.10-4 to
349 11.10-4). In contrast, sequence 4 shows high Ni/Al and Cu/Al ratios (Cu/Al > 20.10-4 and Ni/Al >
350 25.10-4). These higher concentrations of Cu and Ni in TST4 are associated with high TOC value.

351 *0/14-14-76-12W6:*

In this section, TST4 shows a strong increase of Ni/Al ratio from $7.5.10^{-4}$ to 50.10^{-4} and a slight increase of Cu/Al ration from 5.10^{-4} to 9.10^{-4}. No other significant variations are present along this section (Cu/Al ≈ 5.10^{-4} and Ni/Al ≈ $7.5.10^{-4}$).

0/06-33-72-25W5:

This section shows low values for both ratios (Cu/Al ≈ 5.10^{-4} and Ni/Al ≈ $7.5.10^{-4}$), consistent with a more proximal depositional setting dominated by detrital inputs.

Brown Hill:

In sequences 1 and 2, the low Cu/Al and Ni/Al (respectively 6.10^{-4} and 8.10^{-4}) are punctuated by peaks of higher Cu/Al (up to 22.10^{-4}). Along this section, the highest peaks of both ratios are not linked to an important concentration of Ni and Cu but to a very low concentration of Al, it is therefore an artifact of normalization.

Interpretation:

On the four sections, the only significant increase in Cu/Al and Ni/Al ratios occurs during TST4, suggesting a strong increase in organic paleoproductivity during this interval. High amplitude variations of both ratios in this interval also highlight cyclic fluctuations of paleoproductivity during TST4. It is important to note that the increase of the authigenic Ni and Cu occurred after a sharp drop of the sedimentation rates across the boundary between sequence A and B. Even though HST4 present low Ni/Al and Cu/Al ratios, the influence of low sedimentation rates on TST4 enrichment cannot be ruled out. However, it is also worth noting that both Cu and Ni concentrations are positively correlated to Al during sequence A, whereas no such relations were observed in TST4. This evidence supports the hypothesis of a change of nutrient source between sequence A and B, with an increase of primary productivity during TST4. In sequence 3, the small increase of Ni and Cu concentration can be either linked to a small increase of the primary productivity or to a better preservation of the OM (confirmed by U/Th and Mo/Al proxies) at the water sediment interface that will induce a lower recycling of the nutrients included in the OM (Riquier *et al.,* 2005).

4.3.2. Uranium (U), Molybdenum (Mo) and Vanadium (V) variations

Some trace elements present in the water are sensitive to redox condition (e.g. U, Mo, V and Ce) and provide information on the oxygen and sulfur content in the water at the time of the deposition (Emerson and Huested, 1991; Calvert and Pedersen, 1993; Crusius *et al.,* 1996; Brumsack, 2006; Algeo and Lyons, 2006; Tribovillard *et al.,* 2006; Algeo and Tribovillard, 2009).

The **figure 12** presents a cross-plot of the U/Th and V/Cr ratios from four different sections across the basin. In these ratios, the redox-sensitive elements (U and V) are normalized to Th and Cr which are both assumed to be linked to detrital inputs. These ratios therefore present the authigenic variation of U and V that are linked to anoxic episodes. These cross-plots show a link between the ratios and the TOC content along wells 0/16-17-83-25W6 and 0/14-14-76-12W6: samples with high ratios present the highest TOC. These cross-plot also show that sequence 1 and 2 present higher oxygen content (U/Th < 0.75 and V/Cr < 2) than sequence 3 and part of sequence 4 (most of U/Th > 0.75 and V/Cr > 2).

The **figure 13**Error! Reference source not found. presents the vertical evolution of U/Th and Mo/Al along four sections. In the four sections, U/Th ranges from 0.3 to 4.5 whereas the Mo/Al ranges from 1.10^{-4} to 24.10^{-4}.

0/16-17-83-25W6:

From SB1 up to MFS2, both ratios stay low (U/Th ≈ 0.3and Mo/Al ≈ 1.10^{-4}). The interval between MFS2 and SB3 shows an increase, then a decrease of U/Th and Mo/Al ratios (U/Th: from 0.3 up to 1.25 down to 0.3 and Mo/Al: from 1.10^{-4} up to $7.5.10^{-4}$ down to 1.10^{-4}). In sequence 3 the interval presents moderate U/Th (> 0.75) and high Mo/Al (> 5.10^{-4}) that seems to oscillate with no correlation with the transgressive and regressive trends of the sedimentary system. Lastly in the TST4, U/Th and Mo/Al both show significant increases (U/Th: from 0.3 up to 4.5; Mo/Al: from 2.10^{-4} up to 25.10^{-4}).

0/14-14-76-12W6:

Along this section, U/Th and Mo/Al mainly present low values (U/Th < 0.75 and Mo/Al < 5.10^{-4}) except in the TST4 where both ratios increase significantly (up to U/Th ≈ 2.25 and Mo/Al < $15.10^{-4)}$.

0/06-33-72-25W5:

On this section no significant increase of both ratios are present (U/Th < 0.75 and Mo/Al < 5.10^{-4})

Brown Hill:

As for the 0/06-33-72-25W5, both proxies along Brown Hill section show very low values. The only high values of both ratios are linked to very low concentration of Al or Th.

Interpretation:

Figures 12 and 13 present sedimentary records of redox sensitive elements. These figures suggest that the water column was oxic to dysoxic during sequence 1 and 2. In sequence 2, the small increase then decrease of the U/Th and Mo/Al ratios is interpreted as the development of small anoxic puddle in the deepest part of the basin. Above SB3, redox sensitive trace elements suggest variations of O_2 concentrations in the water column and the occurrence of dysoxic to anoxic layers in the deepest part of the basin (located near the well 0/16-17-83-25W6 at that time). In this sequence, the high concentration of Mo suggests that water/sediment interface may contain H_2S (Jones and Manning, 1994). In sequence 4, due to the geodynamic evolution and the changes in the basin physiography, the well 0/16-17-83-25W6 present more proximal deposits. In the TST4, the high U/Th and Mo/Al ratios show the occurrence of anoxic to euxinic conditions. In this interval, O_2-depleted and possible H_2S enriched conditions took place along the more proximal areas. As already mentioned for Ni/Al and Cu/Al ratios, the drop of sedimentary fluxes across the boundary between sequence A and B may influence the dilution of authigenic molybdenum and uranium. However, when corrected from dilution effect based on computed sedimentation rates (dilution 4 times lower in sequence B compared to sequence A), U/Th and Mo/Al ratios are still characteristic of anoxia (respectively 1 and 5.10^{-4}).

4.3.3. Molybdenum (Mo) and TOC variations

Changes in basin restriction can be investigated thanks to molybdenum and TOC covariations. **Figure 14** presents molybdenum versus TOC cross-plot along four sections. On these cross plots, TOC values range from 0 to 15.2 wt%, with the maximums located in the sequence 4 and, the molybdenum concentration ranges from 0 to 101.6 ppm with the maximums located in the sequence 3. The TOC and Mo concentrations from wells 0/14-14-76-12W6 and 0/06-33-72-25W5 and from Brown Hill outcrop stay very low (TOC < 3wt% and Mo < 25) except for two cutting samples located near SB3 and SB4. Mo and TOC covariations in different restricted basins (the Saanich inlet, the Cariaco basin, the Framvaren fjord and the Black sea, respectively SI, CB, FF and BS on **figure 14**) are presented by Algeo and Lyons (2006). All the low TOC and Mo samples of the present cannot be related to one of these case studies. The samples of well 16-17-83-25W6 present more significant results with moderate to high TOC and molybdenum concentration (1.5 < TOC < 15.2 wt% and 0 < Mo < 101.6 ppm). Along this well, values for sequences 1 to 3 fall between the Cariaco basin trend and the Black sea trend, whereas sequence 4 values clearly fall along the Black sea trend.

In restricted basin, due to low water and molybdenum reservoir renewal, the Mo/TOC ratio generally stays low (< 15) whereas in open marine settings, due to the water circulation, the Mo/TOC ratio is relatively high (> 60). The cross-plots of **figure 14** show that regardless of the well and the sequence, samples always presents relatively low Mo/TOC ratios (< 35) which tend to highlight a moderately to highly restricted basin (Algeo and Lyons, 2006). The cross-plots of 0/14-14-76-12W6, 0/06-33-72-25W5 and Brown Hill sections are consistent with **figure 13**: anoxia proxies (U/Th, V/Cr and Mo/Al) do not highlight major anoxic event along those three sections excepted in the early sequence 4 of the 0/14-14-76-12W6 well which induced a low concentration of Mo. Along the well 0/16-17-83-25W6, the interpretation of the basin restriction evolution between sequence A and sequence B must be done with caution: firstly only some intervals of sequence 3 and the TST 4 present anoxia. Secondly, the significant drop of the sedimentary supply across the boundary between sequence 3 and 4 (see **figure 9**) may also impact the concentration of Mo and the TOC. In order to remove this impact, Mo and TOC values from sequence 4 were divided by 4. (which represents the average

sedimentary supply decrease between sequence A and B, Crombez, 2016). This correction puts the sequence 4 samples in the lower left side (with sequences 1 and 2) of the cross plot in an area where a restriction is uncertain. All these observation tends to show that both sequence A and B were deposited in a restricted basin, that may be more restricted in sequence 3 that in the other sequences.

4.3.4. Weathering index of Parker (WIP) and chemical alteration index (CIA) variations

Figure 15 presents a cross-plot of the WIP and CIA along the 0/14-14-76-12W6. On this figure, the WIP ranges from, 20 to 80 but most of the samples are comprised between 35 and 50 whereas the CIA ranges from 45 to 85. This figure does not show any maturity trend along the four sequences. Sediment maturity trend are likely to reveal climatic evolution of an area (Parker, 1970; Nesbitt and Young, 1982; Bahlburg and Dobrzinski, 2011), the cross plot presented in **figure 15** suggests that no major climatic changes took place over the western Canada sedimentary basin during the Lower and Middle Triassic.

5. DISCUSSIONS

In the following section, we discuss the source of OM in the Montney and Doig Formations, the spatial and temporal variations of controlling factors on the accumulation and preservation of this OM and finally, their relationship with relative sea level variations and the basin physiography.

5.1. Organic matter in the Montney and Doig Formations

Rock-Eval analyses show that the OM in the Montney and Doig Formation represents Type II/III source rocks (**figure 3**), which is consistent with the studies of Riediger *et al.* (1990) and Riediger (1997). In the Montney and Doig Formations, two intervals present significant enrichment in OM: the sequence 3 (Upper Montney) and the TST4 (Doig phosphate) which is also consistent with previous studies (Ibrahimbas and Riediger, 2004).

Our Rock-Eval analyses data on extracted, low maturity samples, confirm the presence of kerogen in the studied samples (**figure 4**) whereas palynomorphs analyses (**figure 5**), show that this primary OM derives from planktonic sources. Lastly, the analysis of trace elements shows the occurrence of Cu, Ni, U and Mo enrichments in the Montney and Doig Formations. In the present work, these enrichments are interpreted to be linked to redox conditions and/or primary productivity variations (Tribovillard *et al.,* 2006). As crude oil contains important concentration of trace metal elements (Lord, 1991; Duyck *et al.,* 2002), the enrichments that are highlighted in sequence 3 could also be linked to bitumen associated with secondary cracking of migrated oil. In the present study, we were unable to establish a clear relation between TOC concentration and the trace metal element concentrations, or the Al-normalized concentration of those elements and the TOC. It is therefore unlikely that all the organic content in the Montney Formation comes from migrated hydrocarbons.

In the present work, the study of Rock-Eval S1 values does not allow for the recognition of good conventional reservoir intervals. In the Montney and Doig Formations, average S1 value is low (< 0.4 mgHC/gRock) and high S1 values within low maturity areas, which correspond to good conventional reservoir, are absent. Recent works of Sanei *et al.* (2015) and Wood *et al.* (2015) concluded that most of the organic content in the Montney Formation derives from migrated hydrocarbons. In their studies, the most part of the organic content in the Montney Formation is considered to be pyrobitumen, resulting from the secondary cracking of migrated oil. Regarding the low maturity (Tmax < 450) of the primary organic matter in some part of the basin and the very low permeability of the Montney and Doig Formation (< 0.01 mD, Chalmers and Bustin, 2012), it is unlikely that the organic matter is coming from the secondary cracking of a migrated bitumen (due to the le permeability) or from the secondary cracking of a light oil (due to the low thermic maturity). Our study does not question the presence of pyrobitumen in the Montney-Doig Formations, but it also emphasizes the occurrence of primary kerogen in this interval. Analysis of the elementary proxies shows that the sequence 3 and part of sequence 4 present propitious redox conditions and primary productivity for source rocks development, whereas sequences 1 and 2 present less conductive

conditions to organic rich sediment accumulation (**figure 10 to 13**). Estimating the relative proportion of migrated versus in place hydrocarbons in the Montney Formation is beyond the scope of the present study and would necessitate a quantitative basin analysis.

5.2. Spatial variations and temporal evolution of primary productivity, anoxia and dilution and their impacts on organic matter distribution

Recent works (Sageman *et al.,* 2003; Bohacs *et al.,* 2005; Katz*,* 2005) showed that the organic richness of sedimentary rocks is controlled by a combination of three mains factors: (1) the primary organic production by flora and fauna, (2) its dilution by non-hydrogenated particles and (3) its preservation. Bohacs *et al.* (2005) showed that a high productivity combined with a low dilution rates is not the most efficient way to produce and preserve an organic rich rock. Indeed, an extremely high planktonic productivity will dilute the organic content in the tests of the micro-organisms and a low SR will minimize the burial efficiency and will allow a higher bacterial degradation and oxidation at the water sediment interface and therefore lead to weak preservation.

In the present study, the palynofacies analyses mostly revealed AOM coming from marine planktonic faunas. In a sedimentary basin, the OM can be degraded or destructed by various processes occurring in the water column and in the first centimeters below the water-sediment interface (Demaison and Moore, 1980; Southam *et al.,* 1982; Einsele, 1992; Calvert *et al.,* 1996): (1) In the production areas, the OM produced by micro-organisms can be consumed and recycled by macro-organisms (Eppley and Peterson, 1979). However assuming that the macro organisms also produce OM, this phenomenon only has a small impact on the total OM production. (2) While settling through the water column, the OM can be oxidized and therefore degraded by the oxygen present in the water (Karl *et al.,* 1988; Wakeham and Lee, 1993). Therefore, at a constant production rate, the OM is better preserved in anoxic or dysoxic water (Cowie and Hedges, 1992; Canfield, 1993). However, if production is high enough, sinking OM consume all the oxygen leading to the creation of Oxygen Minimum Zone (OMZ) and the preservation of the remaining OM (Southam *et al.,* 1982; Einsele,

1992; Paulmier and Ruiz-Pino, 2009). (3) In the first centimeter below the water/sediments interface, rapid degradation of the OM takes place as long as oxygen is present. The occurrence of macro-organism in oxic sediments results in bio-degradation of the OM present in the sediments (Ingall *et al.,* 1993). Most of OM degradation will stop a few centimeters below the water/sediments interface due the depletion in oxygen in the buried layers (Wenzhofer and Glud, 2002). Globally, the preservation of OM is highly linked to the oxygen content in the water and sediments.

5.2.1. Basin scale variations of primary productivity, anoxia and dilution

The relative contribution of the three main factors (production-dilution-preservation) controlling initial TOC of sediment can be estimated by integrating sequence stratigraphy interpretation with trace element analysis. Based on trace elements analyses from wells 0/16-17-83-25W6; 0/14-14-76-12W6 and 0/06-33-72-25W5 and based on the Rock-Eval analyses of five additional wells, the **figure 16** presents an interpretation of the vertical and the lateral variations of the factors that drive organic richness in sedimentary rocks. It confirms that there is no simple relation between SR (dilution) and the organic content in the studied interval. Tyson (2001) concluded that SR close to 5 cm/ka may enhance the concentration of the OM which is observable in sequence 1, 2 and the HST4 (**figure 9**).

On the **figure 16**, it is apparent that local OM enrichment occurs near MFS or parasequence flooding surfaces, similar to trends observed by Creaney and Passey (1993). However, a low SR alone cannot explain the organic enrichment of condensed layer, indeed low burial efficiency resulting from a low SR will promote the degradation of OM (Tyson, 2001; Bohacs, 2005; Katz, 2005). In the studied interval, small increases of anoxia proxies are commonly associated with organic rich intervals, suggesting occurrence of small anoxic puddles, most likely linked to basin floor physiography. Local and punctual enrichment would therefore be linked to a combination of starved intervals and local anoxic layers (Algeo and Rowe, 2012).

Figure 16 illustrates that low to moderate organic productivity, mainly oxic water (85% of the U/Th ratio < 0.75, Jones and Manning, 1994) and high sedimentation rates prevailed during sequence 1 and 2, regardless of the position along the depositional profile. In this interval, rare TOC peaks are present and are interpreted to be associated with either local dysoxic to anoxic episodes (U/Th ratio increase) or punctual decrease SR (e.g. near MFS). Above sequence 1 and 2, **figure 16** shows a major change in the paleo-redox conditions. At that time the oxic to dysoxic water of sequence 2 turns into dysoxic to anoxic water marked by an increase of U/Th and Mo/Al ratios (Emerson and Huested, 1991; Tribovillard *et al.,* 2004; Brumsack, 2006). These anoxic conditions are clearly present in the deepest part of the basin, in offshore facies and are weaker in the shoreface facies on the edges on the basin (**figure 16**). This major change of the water's oxygen content is not interpreted to be associated with an important variation of primary productivity. Indeed, the small increases in Cu/Al ratio observed on the 0/16-17-83-25W6 are interpreted to be linked to the better preservation of the OM (Riquier *et al.,* 2005). In sequence 3, the organic-rich deposits are located in the central part of the basin where oxygen content is minimum (**figure 16**). In this interval, the fluctuation of anoxic conditions are associated with the progradation and backstep of the depositional system.

Above this anoxic episode, the **figure 16** shows for the first time an important increase of primary productivity associated with anoxic water marked by important increase of Cu/Al, Ni/Al, U/Th and Mo/Al ratios (Tribovillard *et al.,* 2004; Algeo and Lyons, 2006; Tribovillard *et al.,* 2006). In this interval, organic rich deposits are located in periphery of the basin. Unlike in sequence 3, anoxia is strongest at the edges of the basin and alternate with dysoxic periods, suggesting the onset of an OMZ, triggered by the high primary productivity at sea surface. Above the MFS4, the basin returns to similar conditions as in sequence 1 and 2: low to moderate productivity and high oxygen content in the water, leading to low production and poor preservation of OM (**figure 16**).

5.2.2. Models for organic-rich rocks deposition

In this study, we highlight four main stages characterized by contrasted depositional dynamics that result in different temporal and spatial distributions of OM in the basin:

- Sequence 1 and 2: oxic water and low paleoproductivity.
- Sequence 3: dysoxia/anoxia takes place in the deepest part of the basin.
- TST4: the anoxia is associated with an increase of paleoproductivity on the basin margins.
- Above MSF4, the basin returned to its initial condition: oxic water associated with a low productivity.

Based on these observations we propose a model for the deposition of the organic-rich layer in the Montney and Doig Formations (**figure 17**). These models split the investigated interval in 3 conceptual basin types: Type 1: an oxic basin, that prevailed during sequence 1 and 2 and HST4. Type 2: a restricted basin that is representative of the sequence 3. Type 3: a high primary productivity basin that is diagnostic of the TST4.

During sequence 1, 2 as well as HST4, the low primary productivity along the coast, the high oxygen content in the water lead to limited organic accumulation in the basin (**figure 16 and 17 A**).

In sequence 3, a restriction of the connection between the open marine settings and the basin due to low relative sea level induced a decrease of water circulation and therefore a stratification of the water column that to the development of anoxia in the deepest part of the basin (**figure 16 and 17 B,** Demaison and Moore, 1980; Huc, 1988; Arthur and Sageman, 1994; Brumsack, 2006; Algeo *et al.,* 2008; Algeo and Rowe, 2012). The stratification is supposed to take place below the storm weather wave base (SWWB) where water mixing is limited. This stratification associated with a primary productivity similar to sequence 1 and 2 allows for the preservation of produced OM transported in the deepest part of the basin. On the edges of the basin, where the bathymetry does not go below the SWWB, OM is poorly preserved (**figure 16**).

This study highlighted an increase in primary productivity and the occurrence of anoxic water along the margin of the basin In the TST4 (**figure 16 and 17 C,** Demaison and Moore, 1980; Calvert and Price, 1983; Emeis *et al.,* 1991; Wignall and Newtown, 2001; Brumsack, 2006; Algeo *et al.,* 2008). This

productivity, associated with the anoxia controlled the preservation of very rich organic layers on the edges of the basin. In this systems tract, anoxic condition and increased productivity were also highlighted in the central part of the basin, but with a lower intensity than on the edges of the basin.

The integration of geochemical analyses in the stratigraphic framework highlighted three different types of basin in the studied interval. Those three types of basin present drastically different distribution of OM due to differences in dynamic of anoxia and primary productivity.

Sequence stratigraphy study shows that the deposition of the Montney and Doig Formations most likely took place in an oval shaped basin between the proto-cordillera and the western margin of Pangea (Crombez, 2016; Rohais *et al.,* 2016). In these settings, OM is poorly preserved in type 1 basin (**figure 17 A**). In a type 2 basin (**figure 17 B**), organic rich deposits are located in the central part of the basin where the oxygen content is minimum. This type of basin is very similar to the present-day Black Sea where the production of the OM takes place along the margin of the basin and OM is accumulated in the central part of the basin (Huc, 1988; Wilkin *et al.,* 1997; Arthur and Dean, 1998; Algeo and Lyons, 2006; Algeo *et al.,* 2008). In this type of basin, the organic rich area will likely be round-shaped in the deep basin. Lastly, in a type 3 basin (**figure 17 C**), the organic-rich layers are located below the production areas, where the oxygen content is minimum due to the development of OMZ. As the production areas can be considered a function of the distance to the shore (Calvert, 1987; Baudin *et al.,* 2007), the organic rich areas resulting from this type of basin are likely to be halo-shaped parallel to the shoreline.

5.3. Controls on primary productivity and anoxia

Our analysis suggest that during the Lower and Middle Triassic in Western Canada, the evolution of primary productivity and anoxia through time was associated with major stratigraphic surfaces (**figure 16**). In particular, physiographic changes of the basin across the boundary between third-order sequence 2 and 3 as well as between second-order sequence A and B (Crombez, 2016) appear

to have a major impact on the distribution of organic matter. These changes likely reflect the early geodynamic evolution of the Canadian Cordillera.

5.3.1. Primary productivity

A strong increase of primary productivity occurred during TST4, above a major erosional unconformity that modified the physiography of the basin. Several models explain the increase of organic productivity by an augmentation of nutrients inputs from the continent due to climate enhanced continental weathering (Algeo et al., 2008) or associated with a marine transgression (Wignall and Newton, 2001). Other studies explain the increase of primary productivity by the input of deep marine nutrients associated with upwelling cells (Heckel, 1977; Demaison and Moore, 1980; Calvert and Price, 1983; Emeis et al., 1991).

During sequence A, the positive correlation of detrital supply proxies (Al) with organic productivity proxies (Ni, Cu) suggests that nutrients were supplied by the continent and their low concentration resulted in low to moderate organic productivity in the Montney Formation. During TST4, such a relation between detrital input and organic productivity was not observed, suggesting another source of nutrients. A recent study (Krajewski, 2013) on Triassic strata from Svalbard archipelago, shows that the increase of primary productivity in the basin is mainly controlled by the stratigraphic evolution that establish the connection between upwelling cells and a moderately restricted basin (**figure 14**). A major change of basin physiography across the boundary between sequence A and B, associated with the early geodynamic evolution of the foreland basin might have resulted in the connection with upwelling cells present during the Triassic along the NW margin of Pangea (Parrish and Curtis, 1982). Accordingly, the increase of nutrients delivery during TST4 is probably linked to a combination of the transgressive trend and the regional geodynamic evolution that connect the basin with upwelling cells.

5.3.2. Anoxia

Anoxia in sedimentary basin is mainly driven by two processes: the basin restriction (e.g. the Black Sea, Demaison and Moore, 1980; Huc, 1988; Arthur and Sageman, 1994; Brumsack, 2006; Algeo and Rowe, 2012) and the primary productivity (e.g. the Peruvian Margin, Demaison and Moore, 1980; Arthur and Sageman, 1994; Emeis *et al.,* 1991; Calvert and Price 1983; Arthur and Dean, 1998; Brumsack, 2006; Paulmier and Ruiz-Pino, 2009).

The Montney and Doig Formations present two intervals of anoxia during sequence 3 and TST4. The anoxia in sequence 3 is associated with a moderate to low productivity and a major falling stage of relative sea level whereas TST4 is a second order transgressive period associated with increased primary productivity.

During sequence 3, the lowstand relative sea level lead to restricted connections between the basin and the open marine settings and resulted in reduced water exchange between the two domains and a stratification of the water column. In this setting, the anoxia in the basin is controlled by both the physiography of the basin and the stratigraphic settings that allow for the occurrence of a threshold area.

In the TST4, the high primary productivity triggered the development of an oxygen minimum zone directly below the production area. Unlike in sequence 3, the anoxia in TST4 was controlled by the primary productivity, although the additional impact of basin restriction on anoxia is difficult to estimate.

In the Montney and Doig Formations, the two anoxic episodes present different extension and dynamic. (1) The anoxic episode at the upper part of the Montney Formation was mainly linked to the physiography of the basin and to its stratigraphic evolution. (2) The anoxic areas in TST4 were likely controlled by organic productivity and therefore were not located in the center of the basin but instead in halo-shaped belts associated with up-welling cells. Further work involving forward stratigraphic modeling would help addressing the relative impact of primary productivity versus basin restriction on the resulting anoxia.

6. CONCLUSIONS

The work presented in this paper is based on well and outcrop data. It integrates geochemical analyses in a stratigraphic framework in order to understand the distribution of organic-rich layers in a sedimentary basin and the dynamic of the key controlling factors: primary productivity, dilution and preservation of OM at basin scale. This multidisciplinary study shows:

- The occurrence of primary OM in the Montney and Doig Formations. The palynofacies analyses reveal the occurrence of planktonic OM (**figure 5**).
- The need for a large scale sequence stratigraphic framework to understand local variation of OM accumulation. In the studied interval, the time lines provided the opportunity to understand the major spatial and temporal changes of organic primary productivity and redox conditions.
- The impact of these variations of redox conditions and productivity on the vertical distribution of OM in the Montney and Doig Formations. Sequences 1 and 2 present low TOC content, whereas sequence 3 and TST4 present some organic-rich accumulations. This complex distribution is linked to the development of a “Restricted basin” in sequence 3 and a “High primary productivity basin” in the TST4.
- The lateral variation of OM content due to different rates of productivity and different types of anoxia. In a “High primary productivity basin”, the organic rich layers are located along the coast below the production areas whereas, in a “Restricted basin”, the organic rich layers is deposited in the center basin.
- The occurrence of two different types of anoxia. In the Montney Formation, sequence 1 and 2 may show small episodic “Restricted basins” (ponds) in the basin center and the sequence 3 can be considered as a large “Restricted basin” (**figure 17 B**). In the TST4, the anoxia is located along the basin margin (“High primary productivity basin”, **figure 17 C**). In the Montney Formation, the anoxia is induced by the physiography of the basin and by

the sea level falling stage whereas in the Doig phosphate unit, the anoxia is linked to organic primary productivity associated with a second order transgressive trend induced by major geodynamical changes.

- The primary controls of the basin physiography and stratigraphic settings on anoxia. In the studied interval, the "Restricted basin" is the result of a major sea level falling stage in a threshold basin whereas the "High primary productivity basin" is linked to a major transgressive interval. In the present study, the threshold is linked to the proto-Canadian Cordillera accretion and induces strong restriction.
- The second order transgressive periods do not always present high organic accumulation.
- In our case study anoxia and primary productivity are the two main controls on organic richness, while dilution as only a marginal impact.

ACKNOWLEDGEMENTS

Acknowledgments go to all those who have contributed to this project: IFP Technologies (Canada) Inc., SGS Canada, Alberta Energy regulator and the Geological Survey of Canada. Special acknowledgments go to M.F. Romero Sarmiento, J. Letord, F. Savignac for their help during sample analysis and to Schlumberger that provided Petrel academic licenses.

REFERENCES

Algeo, T.J., Tribovillard, N., 2009. Environmental analysis of paleoceanographic systems based on molybdenum–uranium covariation. Chemical Geology 268, 211–225. doi:10.1016/j.chemgeo.2009.09.001

Algeo, T.J., Lyons, T.W., 2006. Mo-total organic carbon covariation in modern anoxic marine environments: Implications for analysis of paleoredox and paleohydrographic conditions. Paleoceanography 21, n/a–n/a. doi:10.1029/2004PA001112

Algeo, T.J., Rowe, H., 2012. Paleoceanographic applications of trace-metal concentration data. Chemical Geology 324-325, 6–18. doi:10.1016/j.chemgeo.2011.09.002

723 Algeo, T.J., Heckel, P.H., Maynard, J.B., Blakey, R., Rowe, H., 2008. Modern and ancient epeiric seas
724 and the super-estuarine circulation model of marine anoxia. Dynamics of Epeiric seas:
725 sedimentological, paleontological and geochemical perspectives. Geological Association
726 Canada Special Publication 7–38.

727 Armitage, J.H., 1962. Triassic Oil and Gas Occurrences in Northeastern British Columbia, Canada.
728 Bulletin of Canadian Petroleum Geology 10, 35–56.

729 Arthur, M.A., Sageman, B.B., 1994. Marine Black Shales: Depositional Mechanisms and Environments
730 of Ancient Deposits. Annual Review of Earth and Planetary Sciences 22, 499–551.
731 doi:10.1146/annurev.ea.22.050194.002435

732 Arthur, M.A., Dean, W.E., 1998. Organic-matter production and preservation and evolution of anoxia
733 in the Holocene Black Sea. Paleoceanography 13, 395–411. doi:10.1029/98PA01161

734 Bahlburg, H., Dobrzinski, N., 2011. Chapter 6 A review of the Chemical Index of Alteration (CIA) and
735 its application to the study of Neoproterozoic glacial deposits and climate transitions.
736 Geological Society, London, Memoirs 36, 81–92. doi:10.1144/M36.6

737 Baudin, F., Tribovillard, N., Trichet, J., 2007. Géologie de la matière organique. Société géologique de
738 France: Vuibert.

739 Behar, F., Beaumont, V., De B. Penteado, H.L., 2001. Rock-Eval 6 Technology: Performances and
740 Developments. Oil & Gas Science and Technology 56, 111–134.
741 doi:10.2516/ogst:2001013

742 Behar, F., Lorant, F., Lewan, M., 2008. Role of NSO compounds during primary cracking of a Type II
743 kerogen and a Type III lignite. Organic Geochemistry 39, 1–22.
744 doi:10.1016/j.orggeochem.2007.10.007

745 Bohacs, K.M., Carroll, A.R., Mankiewicz, P.J., Miskell-gerhardt, K.J., Schwalbach, J.O.N.R., Wegner,
746 M.B., Simo, J.A.T., 2005. Production, destruction, and dilution-the many paths to source-
747 rock development, in: Harris, N.B. (Ed.), The Deposition Of Organic-Carbon-Rich
748 Sediments : Models, Mechanisms and Consequences. Special Publications of SEPM, pp.
749 61–101.

750 Borisova, A.Y., Freydier, R., Polvé, M., Jochum, K.P., Candaudap, F., 2010. Multi-Elemental Analysis of
751 ATHO-G Rhyolitic Glass (MPI-DING Reference Material) by Femtosecond and
752 Nanosecond LA-ICP-MS: Evidence for Significant Heterogeneity of B, V, Zn, Mo, Sn, Sb,
753 Cs, W, Pt and Pb at the Millimetre Scale. Geostandards and Geoanalytical Research 34,
754 245–255. doi:10.1111/j.1751-908X.2010.00077.x

755 Brumsack, H.-J., 2006. The trace metal content of recent organic carbon-rich sediments: Implications
756 for Cretaceous black shale formation. Palaeogeography, Palaeoclimatology,
757 Palaeoecology 232, 344–361. doi:10.1016/j.palaeo.2005.05.011

758 Calvert, S.E., 1987. Oceanographic controls on the accumulation of organic matter in marine
759 sediments. Geological Society, London, Special Publications 26, 137–151.
760 doi:10.1144/GSL.SP.1987.026.01.08

761 Calvert, S.E., Bustin, R.M., Ingall, E.D., 1996. Influence of water column anoxia and sediment supply
762 on the burial and preservation of organic carbon in marine shales. Geochimica et
763 Cosmochimica Acta 60, 1577–1593. doi:10.1016/0016-7037(96)00041-5

764 Calvert, S.E., Pedersen, T.F., 1993. Geochemistry of Recent oxic and anoxic marine sediments:
765 Implications for the geological record. Marine Geology 113, 67–88. doi:10.1016/0025-
766 3227(93)90150-T

767 Calvert, S., Price, N.B., 1983. Geochemistry of Namibian Shelf Sediments, in: Suess, E., Thiede, J.
768 (Eds.), Coastal Upwelling Its Sediment Record SE - 17, NATO Conference Series. Springer
769 US, pp. 337–375. doi:10.1007/978-1-4615-6651-9_17

770 Canfield, D., 1993. Organic Matter Oxidation in Marine Sediments, in: Wollast, R., Mackenzie, F.,
771 Chou, L. (Eds.), Interactions of C, N, P and S Biogeochemical Cycles and Global Change SE
772 - 14, NATO ASI Series. Springer Berlin Heidelberg, pp. 333–363. doi:10.1007/978-3-642-
773 76064-8_14

774 Catuneanu, O., Galloway, W.E., Kendall, C.G.S.C., Miall, A.D., Posamentier, H.W., Strasser, A., Tucker,
775 M.E., 2011. Sequence Stratigraphy: Methodology and Nomenclature. Newsletters on
776 Stratigraphy 44, 173–245. doi:10.1127/0078-0421/2011/0011

777 Chalmers, G.R.L., Bustin, R.M., 2012. Geological evaluation of Halfway–Doig–Montney hybrid gas
778 shale–tight gas reservoir, northeastern British Columbia. Marine and Petroleum Geology
779 38, 53–72. doi:10.1016/j.marpetgeo.2012.08.004

780 Cowie, G.L., Hedges, J.I., 1992. The role of anoxia in organic matter preservation in coastal sediments:
781 relative stabilities of the major biochemicals under oxic and anoxic depositional
782 conditions. Organic Geochemistry 19, 229–234. doi:10.1016/0146-6380(92)90039-Z

783 Creaney, S., Passey, Q.R., 1993. Recurring Patterns of Total Organic Carbon and Source Rock Quality
784 within a Sequence Stratigraphic Framework. AAPG Bulletin 77, 386–401.

785 Crombez, V., 2016. Petrofacies, sédimentologie et architecture stratigraphique des roches riches en
786 matière organique. Etude multi-approches des formations Montney et Doig (Trias

787 inférieur et moyen, Alberta and Colombie Britannique, Canada). PhD thesis, Université
788 de Paris VI, 238p.

789 Crusius, J., Calvert, S., Pedersen, T., Sage, D., 1996. Rhenium and molybdenum enrichments in
790 sediments as indicators of oxic, suboxic and sulfidic conditions of deposition. Earth and
791 Planetary Science Letters 145, 65–78. doi:10.1016/S0012-821X(96)00204-X
792

793 Davies, G.R., 1997a. The Triassic of the Western Canada Sedimentary Basin: Tectonic and
794 Stratigraphic Framework, Paleogeography, Paleoclimate and Biota. Bulletin of Canadian
795 Petroleum Geology 45, 434–460.

796 Davies, G.R., 1997b. Aeolian Sedimentation and Bypass, Triassic of Western Canada. Bulletin of
797 Canadian Petroleum Geology 45, 624–642.

798 Davies, G.R., Moslow, T.F., Sherwin, M.D., 1997. The Lower Triassic Montney Formation, West-
799 Central Alberta. Bulletin of Canadian Petroleum Geology 45, 474–505.

800 Demaison, G.J., Moore, G.T., 1980. Anoxic Environments and Oil Source Bed Genesis. AAPG Bulletin
801 64, 1179–1209.

802 Ducros, M., Euzen, T., Crombez, V., Sassi, W., Vially, R., n.d. 2-D basin modeling of the WCSB across
803 the Montney-Doig system: implications for hydrocarbon migration pathways and
804 unconventional resources potential, in M. AbuAli and I. Moretti, eds., Petroleum System
805 Case Studies: AAPG Memoir 114. doi: 10.1306/13602027M1143703

806 Duyck, C., Miekeley, N., Porto da Silveira, C.L., Szatmari, P., 2002. Trace element determination in
807 crude oil and its fractions by inductively coupled plasma mass spectrometry using
808 ultrasonic nebulization of toluene solutions. Spectrochimica Acta Part B: Atomic
809 Spectroscopy 57, 1979–1990. doi:10.1016/S0584-8547(02)00171-4

810 Einsele, G., 1992. Sedimentary basins: evolution, facies, and sedimentary budget. Springer-Verlag.

811 Emeis, K.-C., Whelan, J.K., Tarafa, M., 1991. Sedimentary and geochemical expressions of oxic and
812 anoxic conditions on the Peru Shelf. Geological Society, London, Special Publications 58,
813 155–170. doi:10.1144/GSL.SP.1991.058.01.11

814 Emerson, S.R., Huested, S.S., 1991. Ocean anoxia and the concentrations of molybdenum and
815 vanadium in seawater. Marine Chemistry 34, 177–196. doi:10.1016/0304-
816 4203(91)90002-E

817 Eppley, R.W., Peterson, B.J., 1979. Particulate organic matter flux and planktonic new production in
818 the deep ocean. Nature 282, 677–680. doi:10.1038/282677a0

819 Espitalie, J., Deroo, G., Marquis, F., 1986. La pyrolyse Rock-Eval et ses applications. Première partie.
820 Oil & Gas Science and Technology 40, 563–579. doi:10.2516/ogst:1985035

821 Euzen, T., Everett, B., Power, M., Crombez, V., Rohais, S., Vaisblat, N., Baudin, F., 2015. Geological
822 Controls on Reservoir Properties of the Montney Formation in Northeastern BC. An
823 integration of sequence stratigraphy, organic geochemistry, quantitative mineralogy and
824 petrophysical analysis, in: Geoconvention: Geoscience New Horizons. Calgary.

825 Golding, M.L., Mortensen, J.K., Ferri, F., Zonneveld, J.-P., Orchard, M., 2015a. Determining the
826 provenance of Triassic sedimentary rocks in northeastern British Columbia and western
827 Alberta using detrital zircon geochronology, with implications for regional tectonics.
828 Canadian Journal of Earth Sciences. doi:10.1139/cjes-2015-0082

829 Golding, M.L., Orchard, M.J., Zonneveld, J.-P., Wilson, N.S.F., 2015b. Determining the age and
830 depositional model of the Doig Phosphate Zone in northeastern British Columbia using
831 conodont biostratigraphy. Bulletin of Canadian Petroleum Geology 63, 143–170.

832 Gottlieb, P., Wilkie, G., Sutherland, D., Ho-Tun, E., Suthers, S., Perera, K., Jenkins, B., Spencer, S.,
833 Butcher, A., Rayner, J., 2000. Using quantitative electron microscopy for process
834 mineralogy applications. JOM 52, 24–25. doi:10.1007/s11837-000-0126-9

835 Grundman, G., Behar, F., Malo, M., Baudin, F., Lorant, F., 2012. Evaluation of hydrocarbon potential
836 of the Paleozoic (Cambrian–Devonian) source rocks of the Gaspé Peninsula, Québec,
837 Canada: Geochemical characterization, expulsion efficiency, and erosion scenario. AAPG
838 bulletin 96, 729–751.

839 Hallam, A., 1985. A review of Mesozoic climates. Journal of the Geological Society 142, 433–445.
840 doi:10.1144/gsjgs.142.3.0433

841 Haq, B.U., Hardenbol, J., Vail, P.R., 1988. Mesozoic and Cenozoic Chronostratigraphy and Cycles of
842 Sea-Level Change, in: Wilgus, C.K., Hastings, B.S., Kendall, C.G.S.C., Posamentier, H.W.,
843 Ross, J.C., Van Wagoner, J.C. (Eds.), Sea-Level Changes: An Integrated Approach. Special
844 Publications of SEPM.

845 Heckel, P.H., 1977. Origin of phosphatic black shale facies in Pennsylvanian cyclothems of mid-
846 continent North America. AAPG Bulletin 61, 1045–1068.

847 Huc, A.Y., 1988. Aspects of depositional processes of organic matter in sedimentary basins. Organic
848 Geochemistry 13, 263–272. doi:10.1016/0146-6380(88)90045-9

849 Huc, A.Y., Van Buchem, F.S.P., Colletta, B., 2005. Stratigraphic Control on Source-Rock Distribution:
850 First and Second Order Scale, in: Harris, N.B. (Ed.), . Special Publications of SEPM, pp.
851 225–242.

852 Ibrahimbas, A., Riediger, C., 2004. Hydrocarbon source rock potential as determined by Rock-Eval
853 6/TOC pyrolysis, northeast British Columbia and Northwest Alberta, Resource
854 Development and Geosciences Banch, Sumary of Activities 2004.

855 Ingall, E.D., Bustin, R.M., Van Cappellen, P., 1993. Influence of water column anoxia on the burial and
856 preservation of carbon and phosphorus in marine shales. Geochimica et Cosmochimica
857 Acta 57, 303–316. doi:10.1016/0016-7037(93)90433-W

858 Jarvie, D.M., 2012. Shale Resource Systems for Oil and Gas: Part 1—Shale-gas Resource Systems 69–
859 87. doi:10.1306/13321446M973489

860 Jarvie, D.M., Hill, R.J., Ruble, T.E., Pollastro, R.M., 2007. Unconventional shale-gas systems: The
861 Mississippian Barnett Shale of north-central Texas as one model for thermogenic shale-
862 gas assessment. AAPG bulletin 91, 475–499.

863 Jones, B., Manning, D.A.C., 1994. Comparison of geochemical indices used for the interpretation of
864 palaeoredox conditions in ancient mudstones. Chemical Geology 111, 111–129.
865 doi:10.1016/0009-2541(94)90085-X

866 Karl, D.M., Knauer, G.A., Martin, J.H., 1988. Downward flux of particulate organic matter in the
867 ocean: a particle decomposition paradox. Nature 332, 438–441. doi:10.1038/332438a0

868 Katz, B.J., 2005. Controlling Factors on Source Rock Development—A Review of Productivity,
869 Preservation, and Sedimentation Rate, in: Harris, N.B. (Ed.), The Deposition Of Organic-
870 Carbon-Rich Sediments : Models, Mechanisms and Consequences. Special Publications
871 of SEPM, pp. 7–16.

872 Krajewski, K.P., 2013. Organic matter–apatite–pyrite relationships in the Botneheia Formation
873 (Middle Triassic) of eastern Svalbard: Relevance to the formation of petroleum source
874 rocks in the NW Barents Sea shelf. Marine and Petroleum Geology 45, 69–105.
875 doi:10.1016/j.marpetgeo.2013.04.016

876 Lord, C.J., 1991. Determination of trace metals in crude oil by inductively coupled plasma mass
877 spectrometry with microemulsion sample introduction. Analytical Chemistry 63, 1594–
878 1599. doi:10.1021/ac00015a018

McLennan, S.M., 2001. Relationships between the trace element composition of sedimentary rocks and upper continental crust. Geochemistry, Geophysics, Geosystems 2, n/a–n/a. doi:10.1029/2000GC000109

Monger, J., Price, R., 2002. The Canadian cordillera: Geology and Tectonic Evolution. CSEG Recorder 27, 17–36.

Myers, K.J., 1996. Organic-Rich Facies and Hydrocarbon Source Rocks, in: Sequence Stratigraphy. Blackwell Publishing Ltd., pp. 238–257. doi:10.1002/9781444313710.ch11

Nesbitt, H.W., Young, G.M., 1982. Early Proterozoic climates and plate motions inferred from major element chemistry of lutites. Nature 299, 715–717. doi:10.1038/299715a0

Orchard, M.J., Zonneveld, J.-P., 2009. The Lower Triassic Sulphur Mountain Formation in the Wapiti Lake area: lithostratigraphy, conodont biostratigraphy, and a new biozonation for the lower Olenekian (Smithian). Candian Journal of Earth Sciences 46, 757–790.

Parker, A., 2009. An Index of Weathering for Silicate Rocks. Geological Magazine 107, 501. doi:10.1017/S0016756800058581

Parrish, J.T., Curtis, R.L., 1982. Atmospheric circulation, upwelling, and organic-rich rocks in the Mesozoic and Cenozoic eras. Palaeogeography, Palaeoclimatology, Palaeoecology 40, 31–66. doi:10.1016/0031-0182(82)90084-0

Paulmier, A., Ruiz-Pino, D., 2009. Oxygen minimum zones (OMZs) in the modern ocean. Progress in Oceanography 80, 113–128. doi:10.1016/j.pocean.2008.08.001

Riediger, C.L., Brooks, P.W., Fowler, M.G., Snowdon, L.R., 1990. Lower and Middle Triassic source rocks, thermal maturation, and oil-source rock correlations in the Peace River Embayment area, Alberta and British Columbia. Bulletin of Canadian Petroleum Geology 38, 218–235.

Riediger, C.L., 1997. Geochemistry of Potential Hydrocarbon Source Rocks of Triassic Age in the Rocky Mountain Foothills of Northeastern British Columbia and West-Central Alberta. Bulletin of Canadian Petroleum Geology 45, 719–741.

Riquier, L., Tribovillard, N., Averbuch, O., Joachimski, M.M., Racki, G., Devleeschouwer, X., El albani, A., Riboulleau, A., 2005. Understanding Late Devonian And Permian-Triassic Biotic and Climatic Events - Towards an Integrated Approach, Developments in Palaeontology and Stratigraphy, Developments in Palaeontology and Stratigraphy. Elsevier. doi:10.1016/S0920-5446(05)80008-1

910 Rohais, S., Crombez, V., Euzen, T., Baudin, F., 2016. The Montney-Doig-Halfway Formations from
911 Western Canadian Sedimentary Basin (WCSB): Passive margin, Back-Arc or Fore-Arc
912 geodynamic setting?, in: Geoconvention: Optimizing Resources. Calgary.

913 Rokosh, C.D., Lyster, S., Anderson, S.D.A., Beaton, A.P., Berhane, H., Brazzoni, T., Chen, D., Cheng, Y.,
914 Mack, T., Pana, C., Pawlowicz, J.G., 2012. Summary of Alberta's Shale- and Siltstone-
915 Hosted Hydrocarbon Resource Potential. Energy Resources Conservation Board.

916 Romero-Sarmiento, M.-F., Euzen, T., Rohais, S., Jiang, C., Littke, R., 2016. Artificial thermal maturation
917 of source rocks at different thermal maturity levels: Application to the Triassic Montney
918 and Doig Formation in the Western Canada Sedimentary Basin. Organic geochemistry
919 97, 148-162. doi:10.1016/j.orggeochem.2016.05.002

920 Sageman, B.B., Murphy, A.E., Werne, J.P., Ver Straeten, C.A., Hollander, D.J., Lyons, T.W., 2003. A tale
921 of shales: the relative roles of production, decomposition, and dilution in the
922 accumulation of organic-rich strata, Middle–Upper Devonian, Appalachian basin.
923 Chemical Geology 195, 229–273. doi:10.1016/S0009-2541(02)00397-2

924 Sanei, H., Haeri-Ardakani, O., Wood, J.M., Curtis, M.E., 2015. Effects of nanoporosity and surface
925 imperfections on solid bitumen reflectance (BRo) measurements in unconventional
926 reservoirs. International Journal of Coal Geology 138, 95–102.
927 doi:10.1016/j.coal.2014.12.011

928 Schoepfer, S.D., Shen, J., Wei, H., Tyson, R. V., Ingall, E., Algeo, T.J., 2014. Total organic carbon,
929 organic phosphorus, and biogenic barium fluxes as proxies for paleomarine productivity.
930 Earth-Science Reviews 149, 23–52. doi:10.1016/j.earscirev.2014.08.017

931 Schwarzkopf, T.A., 1993. Model for prediction of organic carbon content in possible source rocks.
932 Marine and Petroleum Geology 10, 478–492. doi:10.1016/0264-8172(93)90049-X

933 Sellwood, B.W., Valdes, P.J., 2006. Mesozoic climates: General circulation models and the rock
934 record. Sedimentary Geology 190, 269–287. doi:10.1016/j.sedgeo.2006.05.013

935 Slatt, R.M., Rodriguez, N.D., 2012. Comparative sequence stratigraphy and organic geochemistry of
936 gas shales: Commonality or coincidence? Journal of Natural Gas Science and Engineering
937 8, 68–84. doi:10.1016/j.jngse.2012.01.008

938 Southam, J.R., Peterson, W.H., Brass, G.W., 1982. Dynamics of anoxia. Palaeogeography,
939 Palaeoclimatology, Palaeoecology 40, 183–198. doi:10.1016/0031-0182(82)90089-X

940 Taylor, S.R., McLennan, S.M., 1985. The continental crust: Its composition and evolution.

941 Tommeras, A., Mann, U., 2008. Improved hydrocarbon charge prediction by source-rock modelling.
942 Petroleum Geoscience 14, 291–299. doi:10.1144/1354-079308-766

943 Tribovillard, N., Algeo, T.J., Lyons, T., Riboulleau, A., 2006. Trace metals as paleoredox and
944 paleoproductivity proxies: An update. Chemical Geology 232, 12–32.
945 doi:10.1016/j.chemgeo.2006.02.012

946 Tribovillard, N., Riboulleau, A., Lyons, T., Baudin, F., 2004. Enhanced trapping of molybdenum by
947 sulfurized marine organic matter of marine origin in Mesozoic limestones and shales.
948 Chemical Geology 213, 385–401. doi:10.1016/j.chemgeo.2004.08.011

949 Tyson, R. V, 1995. Sedimentary organic matter: organic facies and palynofacies. London, New York.

950 Tyson, R.V., 2001. Sedimentation rate, dilution, preservation and total organic carbon: some results
951 of a modelling study. Organic Geochemistry 32, 333–339. doi:10.1016/S0146-
952 6380(00)00161-3

953 Van Buchem, F.S.P., Pradier, B., Stefani, M., 2005. Stratigraphic Patterns in Carbonate Source-Rock
954 Distribution: Second-Order to Fourth-Order Control and Sediment Flux, in: Harris, N.B.
955 (Ed.), The Deposition Of Organic-Carbon-Rich Sediments : Models, Mechanisms and
956 Consequences. Special Publications of SEPM, pp. 191–224.

957 Wakeham, S., Lee, C., 1993. Production, Transport, and Alteration of Particulate Organic Matter in
958 the Marine Water Column, in: Engel, M., Macko, S. (Eds.), Organic Geochemistry SE - 6,
959 Topics in Geobiology. Springer US, pp. 145–169. doi:10.1007/978-1-4615-2890-6_6

960 Wenzhöfer, F., Glud, R.N., 2004. Small-scale spatial and temporal variability in coastal benthic O 2
961 dynamics: Effects of fauna activity. Limnology and Oceanography 49, 1471–1481.
962 doi:10.4319/lo.2004.49.5.1471

963 Whitfield, M., 2001. Advances in Marine Biology V41, Advances in Marine Biology. Elsevier.
964 doi:10.1016/S0065-2881(01)41002-9

965 Wignall, P.B., Newton, R., 2001. Black shales on the basin margin: a model based on examples from
966 the Upper Jurassic of the Boulonnais, northern France. Sedimentary Geology 144, 335–
967 356. doi:10.1016/S0037-0738(01)00125-7

968 Wignall, P.B., 1991. Model for transgressive black shales? Geology 19, 167–170. doi:10.1130/0091-
969 7613(1991)019

Wilkin, R., Arthur, M., Dean, W., 1997. History of water-column anoxia in the Black Sea indicated by pyrite framboid size distributions. Earth and Planetary Science Letters 148, 517–525. doi:10.1016/S0012-821X(97)00053-8

Wood, J.M., Sanei, H., Curtis, M.E., Clarkson, C.R., 2015. Solid bitumen as a determinant of reservoir quality in an unconventional tight gas siltstone play. International Journal of Coal Geology. doi:10.1016/j.coal.2015.03.015

Zonneveld, J.-P., MacNaughton, R.B., Utting, J., Beatty, T.W., Pemberton, S.G., Henderson, C.M., 2010. Sedimentology and Ichnology of the Lower Triassic Montney Formation in the Pedigree-Ring/Border-Kahntah River Area, Northwestern Alberta and Northeastern British Columbia. Bulletin of Canadian Petroleum Geology 58, 115–140.

FIGURES CAPTIONS

Figure 1: Location map of the data available for this study. The names 0/06-33, 0/14-14 and 0/16-17, respectively stand for wells: 0/06-33-72-25W5, 0/14-14-76-12W6 and 0/16-17-83-25W6. The map on the upper right side indicates the location of the study area within the Western Canada sedimentary basin and the Montney Formation subcrop area. BC – British Columbia; AB – Alberta; CC – Canadian Cordillera; WCSB – Western Canada Sedimentary Basin; CS – Canadian Shield; UC – Ursula Creek outcrop; BH – Brown Hill outcrop.

Figure 2: Simplified sedimentary architecture of the Lower and Middle Triassic strata of the Western Canada sedimentary basin (modified from Crombez, 2016). On this sketch, the Brown Hill outcrop (BH) located near to Williston Lake in the fold and thrust belt of the Canadian Cordillera, was moved to its estimated original position at the time of deposition. TST – Transgressive systems tract; HST – Highstand systems tract; FSST – Falling stage systems tract; LST – Lowstand systems tract.

Figure 3: A. HI vs Tmax cross-plots for core samples with TOC values. B. HI vs Tmax cross-plots for cuttings samples with TOC values. These figures show that most of the OM in the Montney and Doig Fm is Type II and Type III. Here, the increase of the TOC with the maturity is biased by the data sampling: in the basin the most mature areas contain the richest samples. HI – Hydrogen index.

Figure 4: FID curves from the Basic Rock–Eval pyrolysis of an early mature cutting sample before and

after hydrocarbons (HC) extraction with organic solvent. HC extraction highlighted the presence of heavy HC in the S2 peak. FID - Flame Ionization Detector; BR – Bulk Rock; eBR – Extracted Bulk Rock.

Figure 5: Palynofacies view of the Montney and Doig Fm. showing that most of the primary OM of the studied interval is amorphous. On these pictures only few terrestrial particles (spores, pollen grains or woody debris) are present and no damaged terrestrial particles can be observed. PM – Palynomaceral = Terrestrial organic matter; SP – Spore/Pollen; AOM – Amorphous organic matter; Py – Pyrite.

Figure 6: Well section across the Montney and Doig Fm with TOC measurements and estimations of the TOC_{ini} for two initial Hydrogen index (IH_{ini} = 350 and IH_{ini} = 600) in a stratigraphic framework. This **figure** shows that the organic content of sequence 3 and 4 is higher than in sequence 1 and 2.

Figure 7: Distribution of the TOC and computed TOC_{ini} in the studied interval and in the four sequences. Solid bars represent actual TOC and hatched bars represent TOC_{in}. It shows that the mean TOC in the studied interval is 1.28 wt% and present heterogeneities: the TOC content of sequence 3 and TST4 is higher than the content of sequence 1 and 2.

Figure 8: Sedimentary section of sequences 3 and 4 from the core description of the 0/16-17-83-25W6. This figure shows that low energy facies were dominant in the LST3 whereas during the TST4 high energy facies are dominant.

Figure 9: Cross-plots of the TOC_{ini} and the SR. Here, SR are based on undecompacted sediments. White symbols show intervals where SR may be underestimated due to an erosional top. These cross-plots, present two types of relation between TOC_{ini} and SR. In sequence 1, 2 and HST4 a linear relation exists between TOC_{ini} and SR that reflect organic dilution by non-organic sediments. In sequence 3 and TST4, this relation is not evident which suggests others controls on organic accumulation and preservation.

Figure 10: Cross-plots of the enrichment factors (EF) of Ni and Cu. The EF are computed based on the UCC (McLennan, 2001). Red lines in the cross-plots represent the Upper Continental Crust. This figure

1022 shows that paleoproductivity increased significantly in the TST4 whereas it remains stable in the rest
1023 of the studied interval.

1024 **Figure 11:** Vertical evolution of paleoproductivity proxies (Cu/Al and Ni/Al) in relation to TOC and
1025 TOC_{ini}. This figure shows that paleoproductivity increased significantly in the TST4 and that along
1026 Brown Hill, small increases of Ni/Al often occur is sequence 2, but no increases in TOC can be related
1027 to these peaks.

1028 **Figure 12:** Cross-plots of paleoredox proxies (U/Th and V/Cr). Limit values between
1029 oxic/dysoxic/anoxic domains are from Jones and Manning (1994). This figure shows the occurrence
1030 of anoxic layers in sequence 3 and 4.

1031 **Figure 13:** Vertical evolution of paleoredox proxies (U/Th and Mo/Al) in relation to TOC and TOC_{ini} in
1032 the stratigraphic framework. This figure shows a major change above the SB3 and above the
1033 TS4/SB4. During sequence 3, the basin seems to be anoxic in its deepest parts whereas in the TST4,
1034 the basin presents anoxia to euxinia along its margin.

1035 **Figure 14**: Cross-plot of the molybdenum versus the TOC in the stratigraphic framework. This figure
1036 shows that in the Lower and Middle Triassic strata of the western Canada sedimentary basin, the
1037 Mo/TOC ratio is low ($< 30.10^{-4}$) which suggests a basin restriction. SA: Saanich inlet; CB: Cariaco
1038 basin; FF: Framvaren fjord; BS: Black sea. Grey arrows highlight the potential effect of maturity on
1039 TOC values.

1040 **Figure 15:** Cross-plot of the weathering index of Parker (WIP) and the chemical index of alteration
1041 (CIA) in the stratigraphic framework. This cross-plot suggests that no major change of sediment
1042 maturity occurred during the Lower and Middle Triassic strata of the western Canada sedimentary
1043 basin.

1044 **Figure 16:** TOC distribution and its controlling factors. This figure shows that high TOC values may
1045 result from different combinations of controlling factors

Figure 17: Conceptual models of basin types proposed for the controls of organic matter accumulations in the Lower and Middle Triassic of Western Canada. A. Type1: Oxic basin, with low OM accumulation. B. Type 2: Restricted basin, with the occurrence of organic rich layer in the central part of the basin due to stratified water. C. Type 3: High primary productivity basin, with the occurrence of organic rich intervals along the proximal parts of the basin due to high productivity.

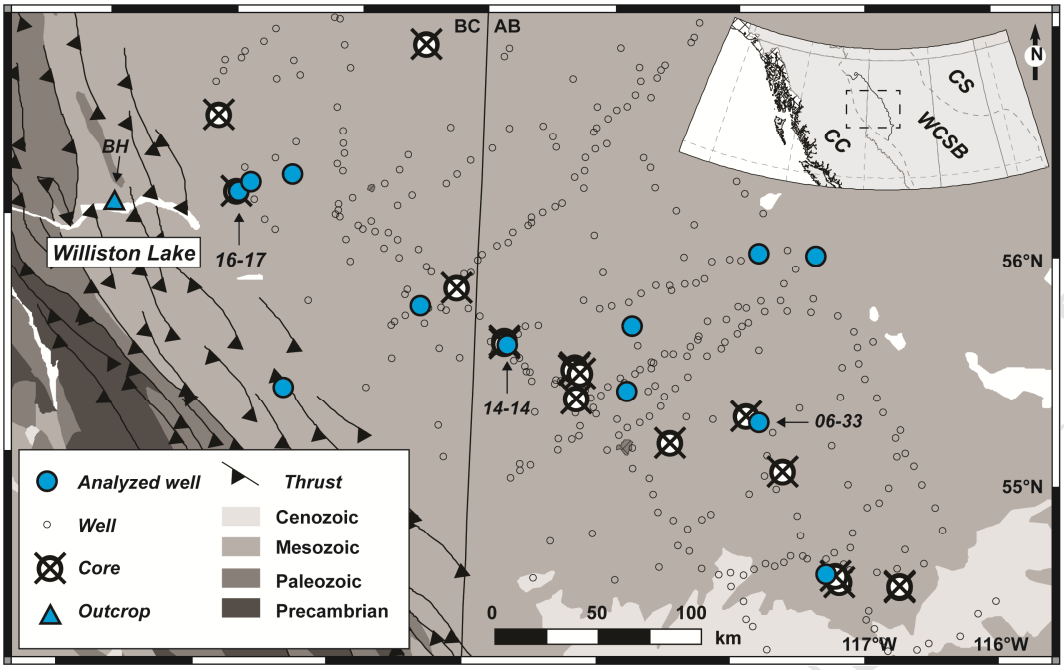

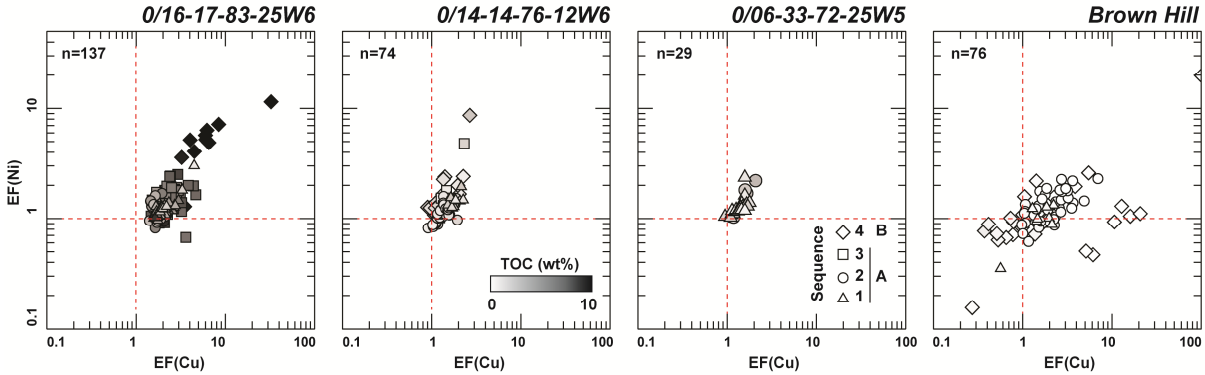

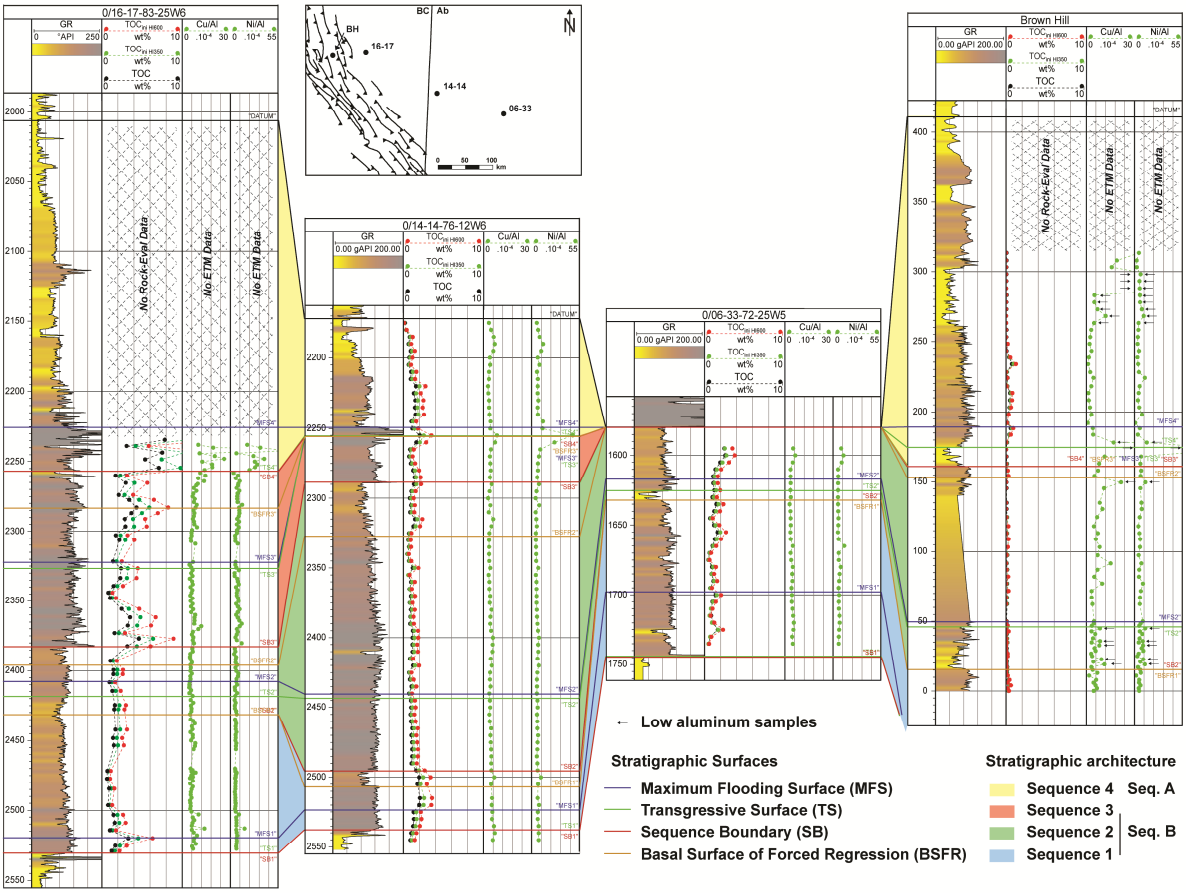

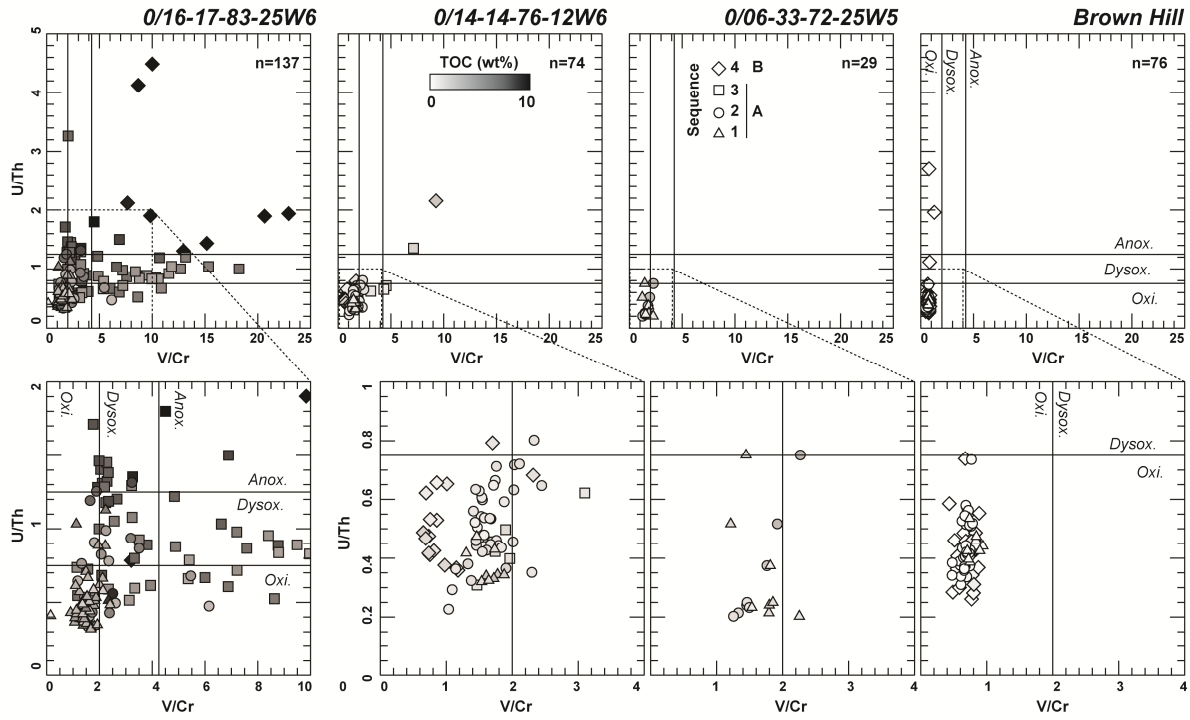

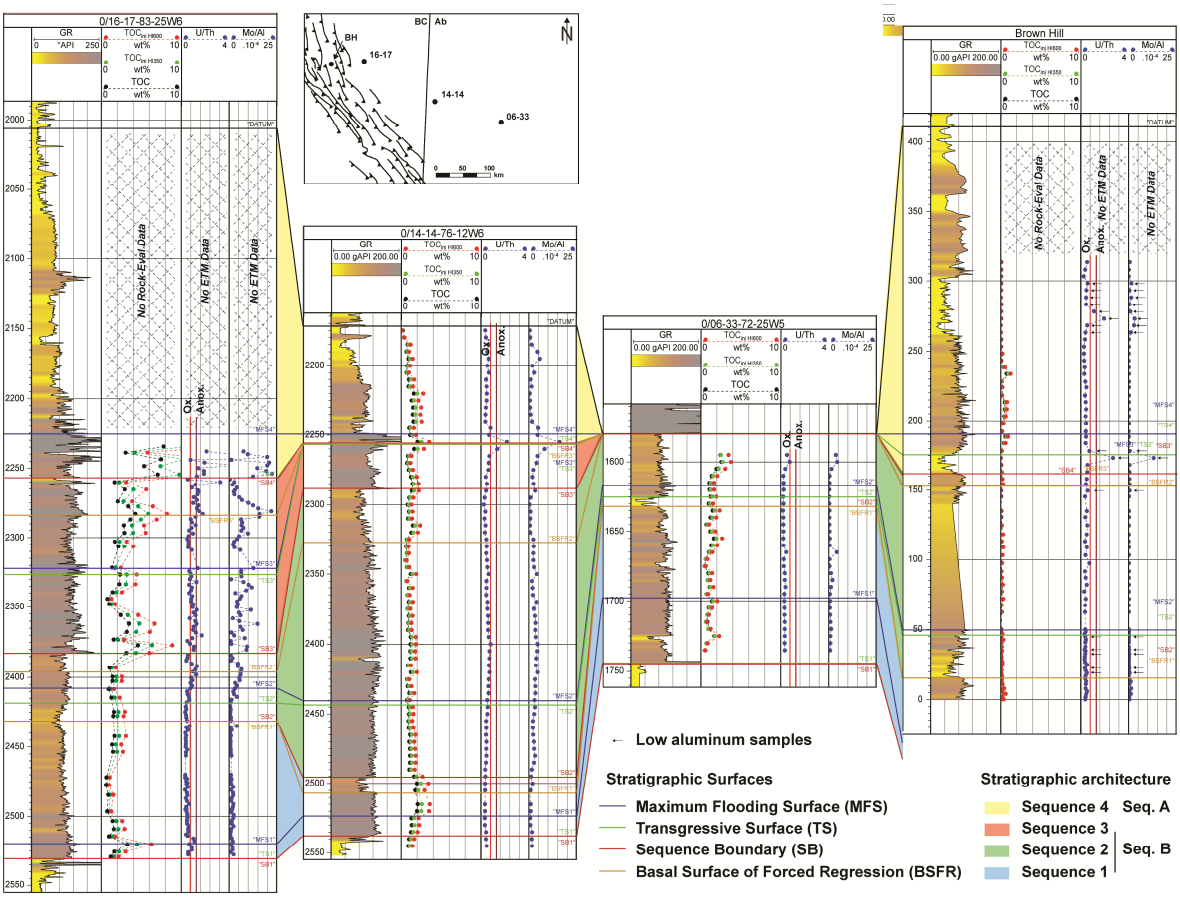

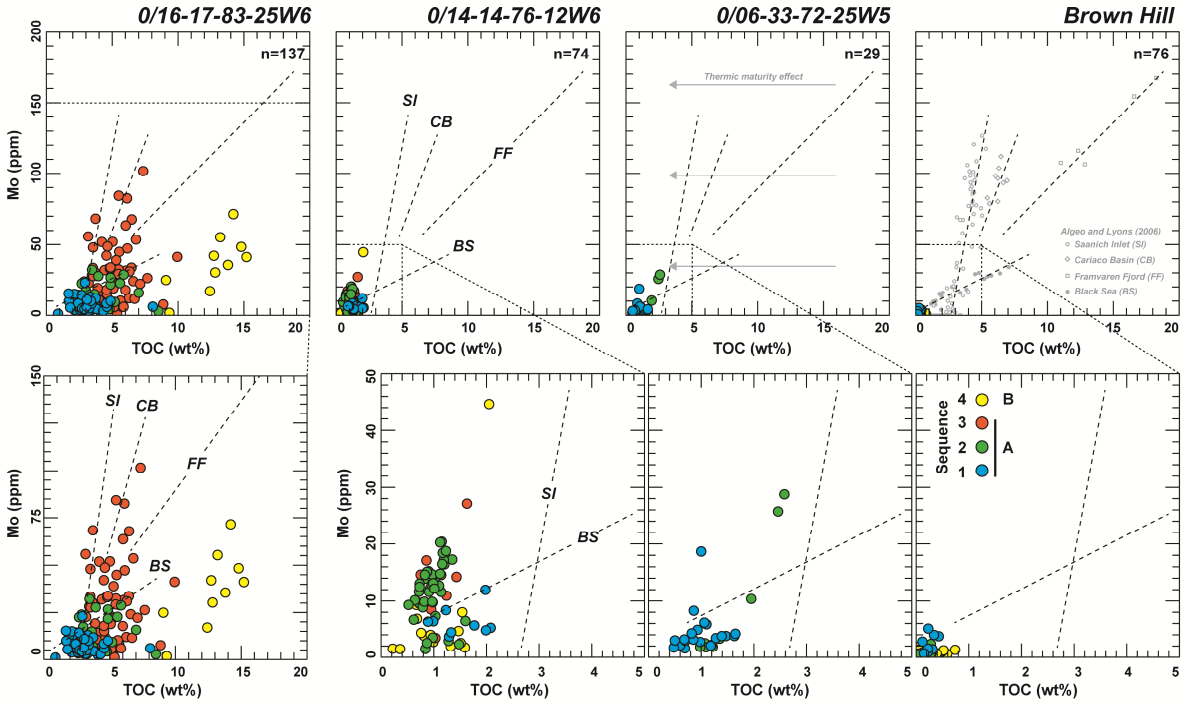

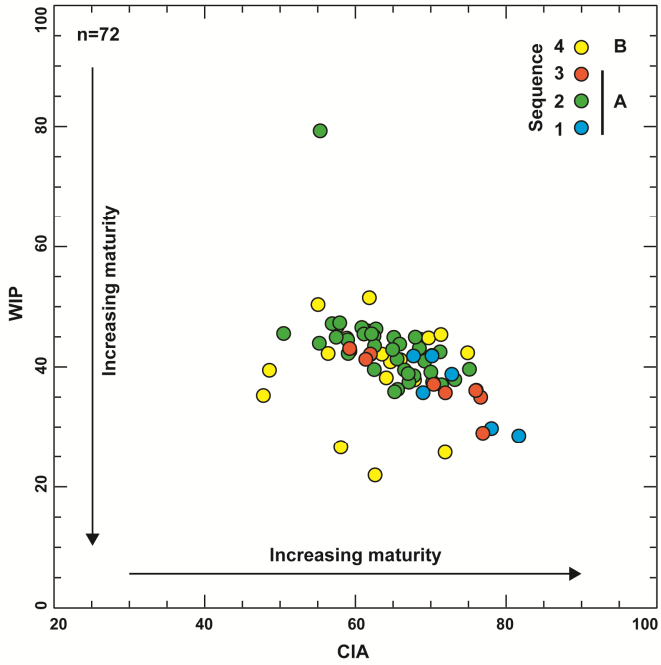

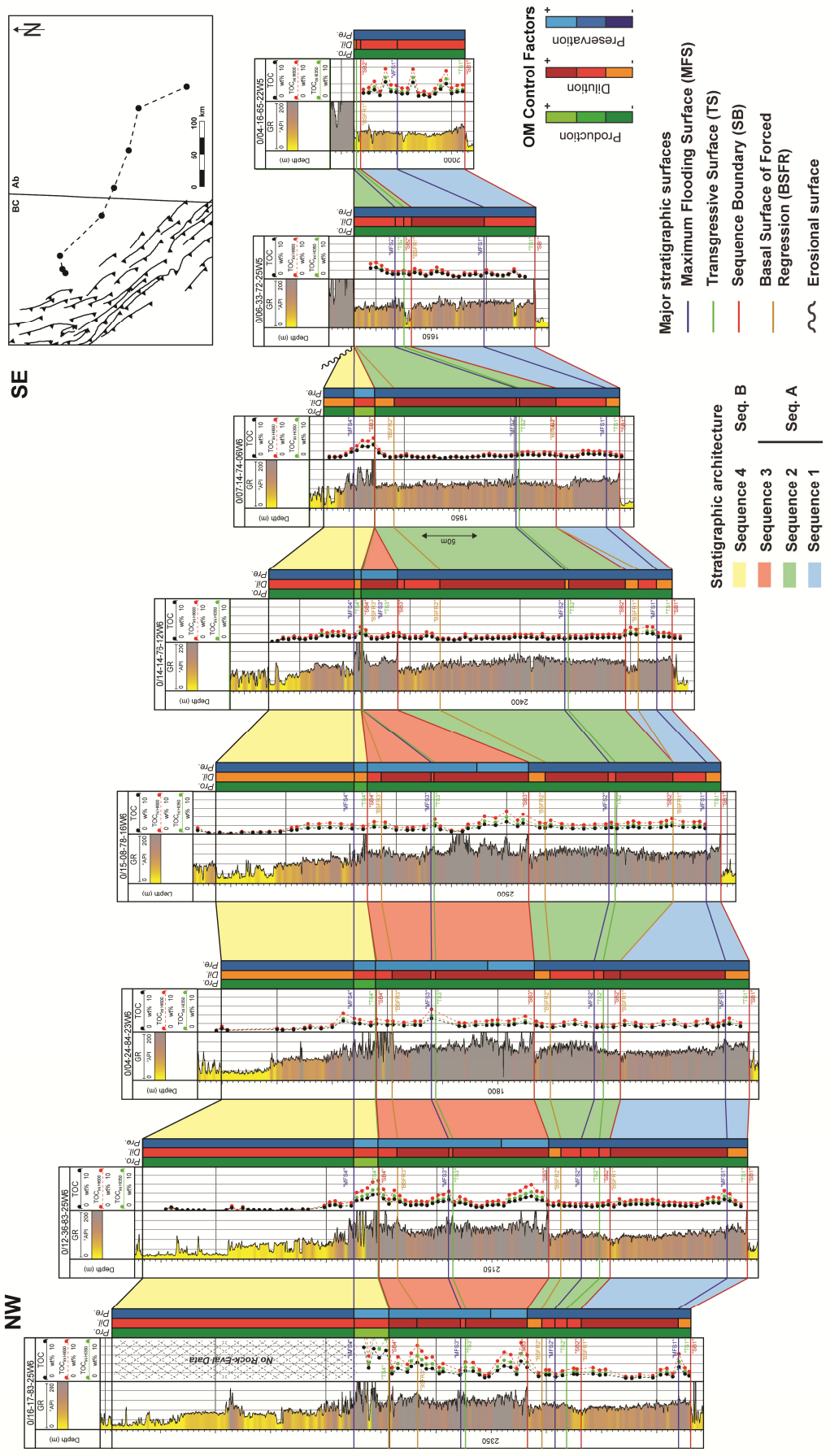

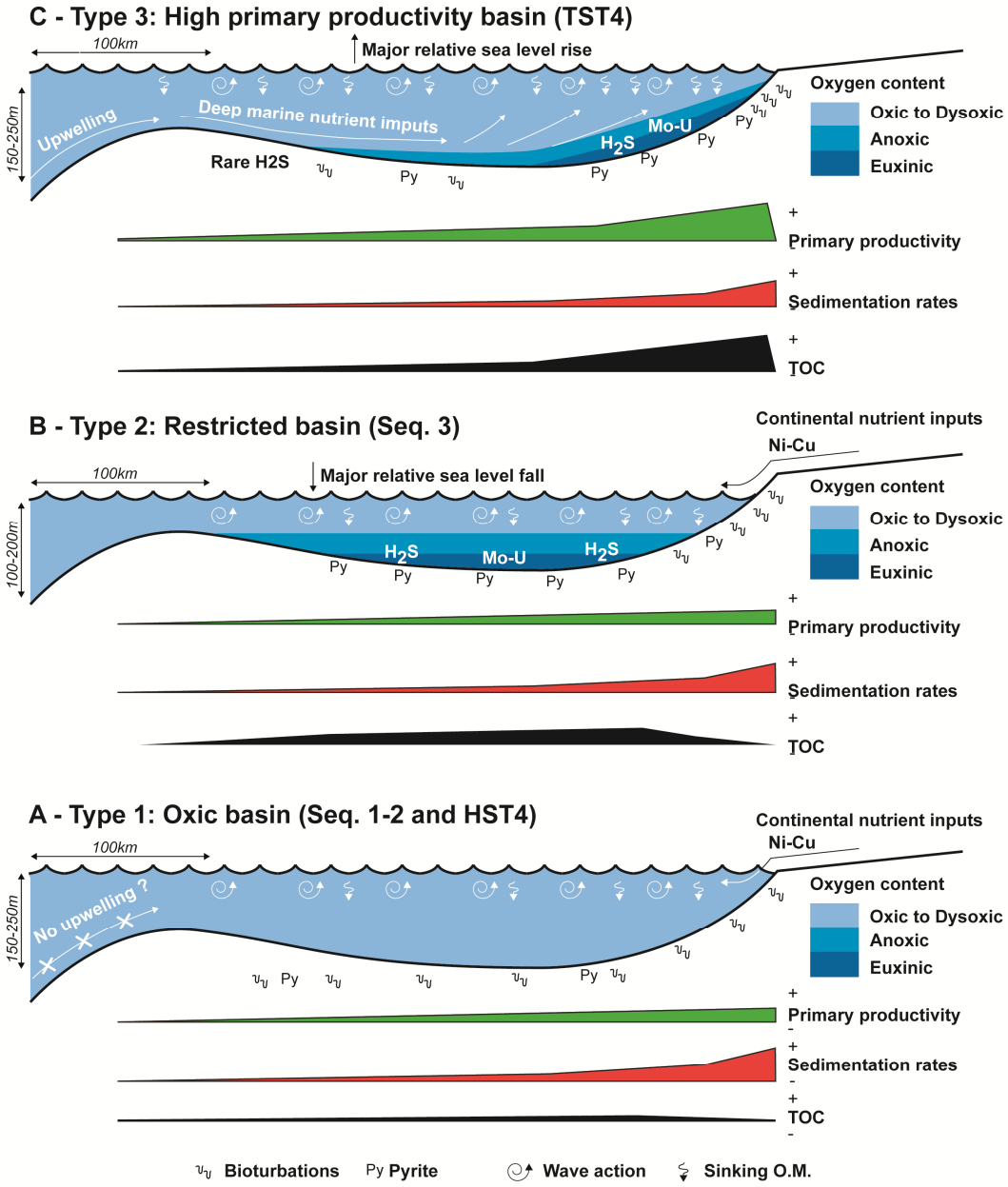
C - Type 3: High primary productivity basin (TST4)
100km
Major relative sea level rise
150-250m
Upwelling
Deep marine nutrient imputs
Rare H2S
H2S
Mo-U
Py
Oxygen content
Oxic to Dysoxic
Anoxic
Euxinic
+
Primary productivity
+
Sedimentation rates
+
TOC
B - Type 2: Restricted basin (Seq. 3)
Continental nutrient inputs
Ni-Cu
100km
Major relative sea level fall
100-200m
H2S
Mo-U
H2S
Py
Oxygen content
Oxic to Dysoxic
Anoxic
Euxinic
+
Primary productivity
+
Sedimentation rates
+
TOC
A - Type 1: Oxic basin (Seq. 1-2 and HST4)
Continental nutrient inputs
Ni-Cu
100km
150-250m
No upwelling ?
Py
Oxygen content
Oxic to Dysoxic
Anoxic
Euxinic
+
Primary productivity
-
+
Sedimentation rates
-
+
TOC
-
Bioturbations
Py Pyrite
Wave action
Sinking O.M.

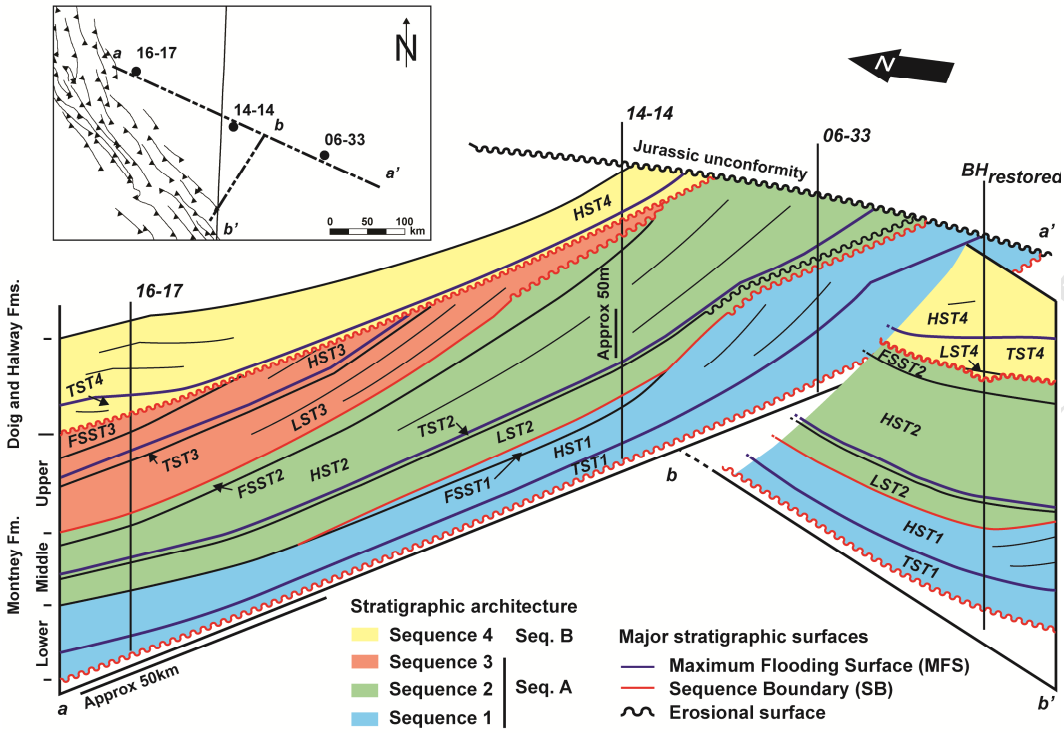

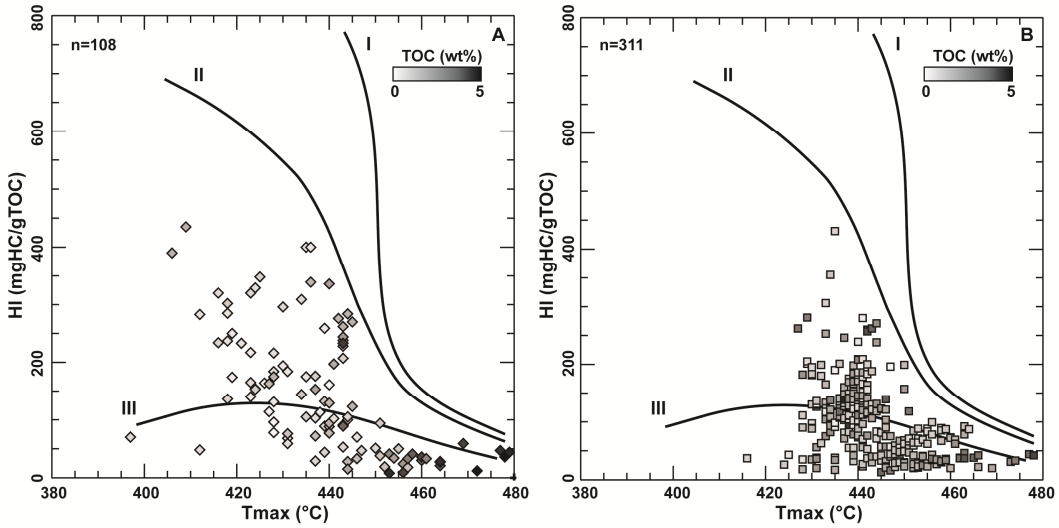

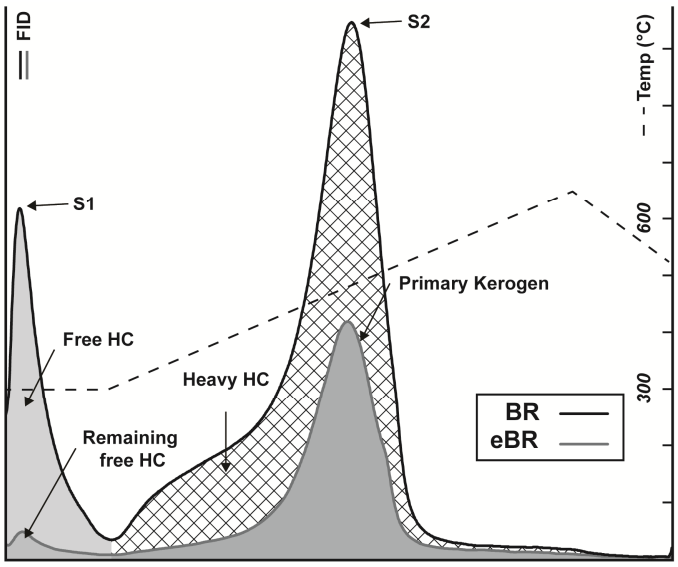

	(mgHC/gTOC)		(°C)	(%)
	S1	S2	Tmax	TOC
BR	0.46	1.96	443	1.05
eBR	0.07	1.40	439	0.92

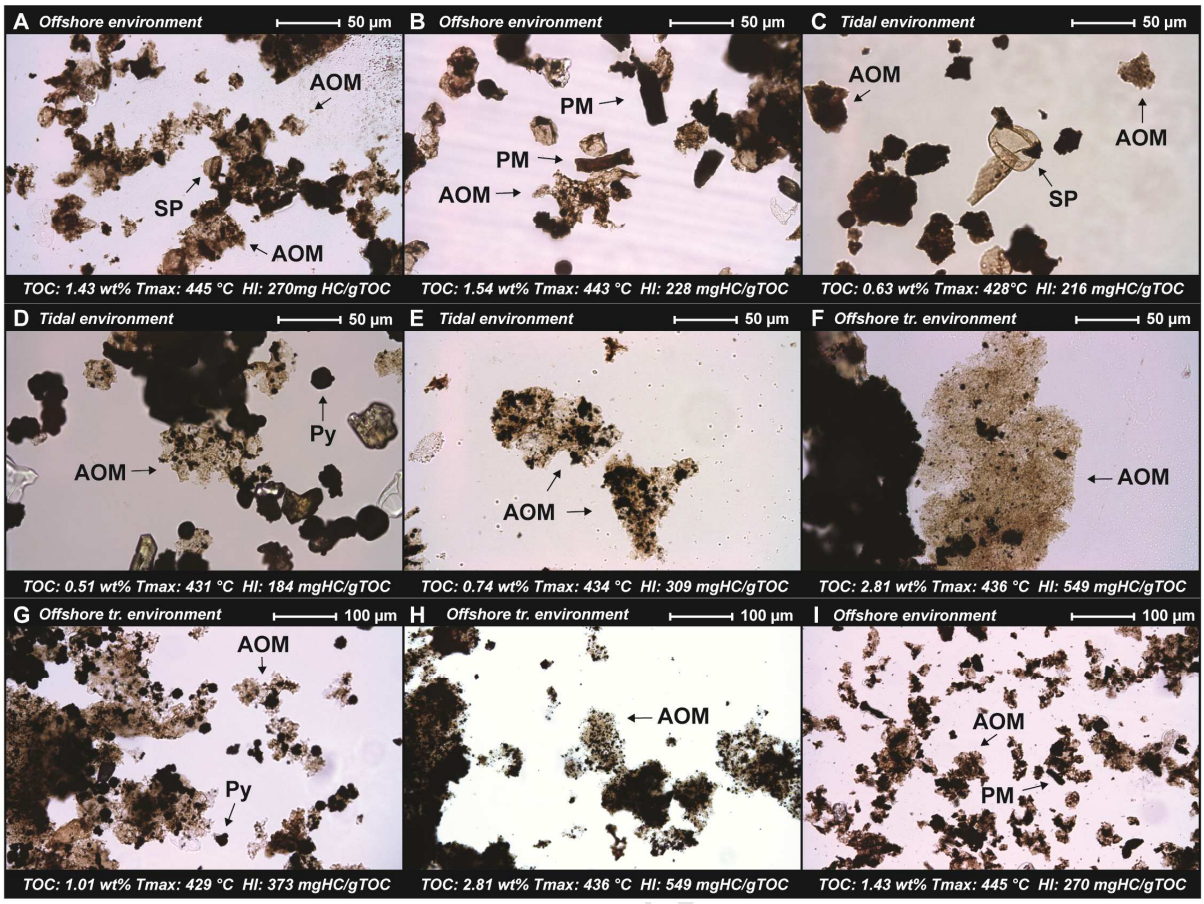

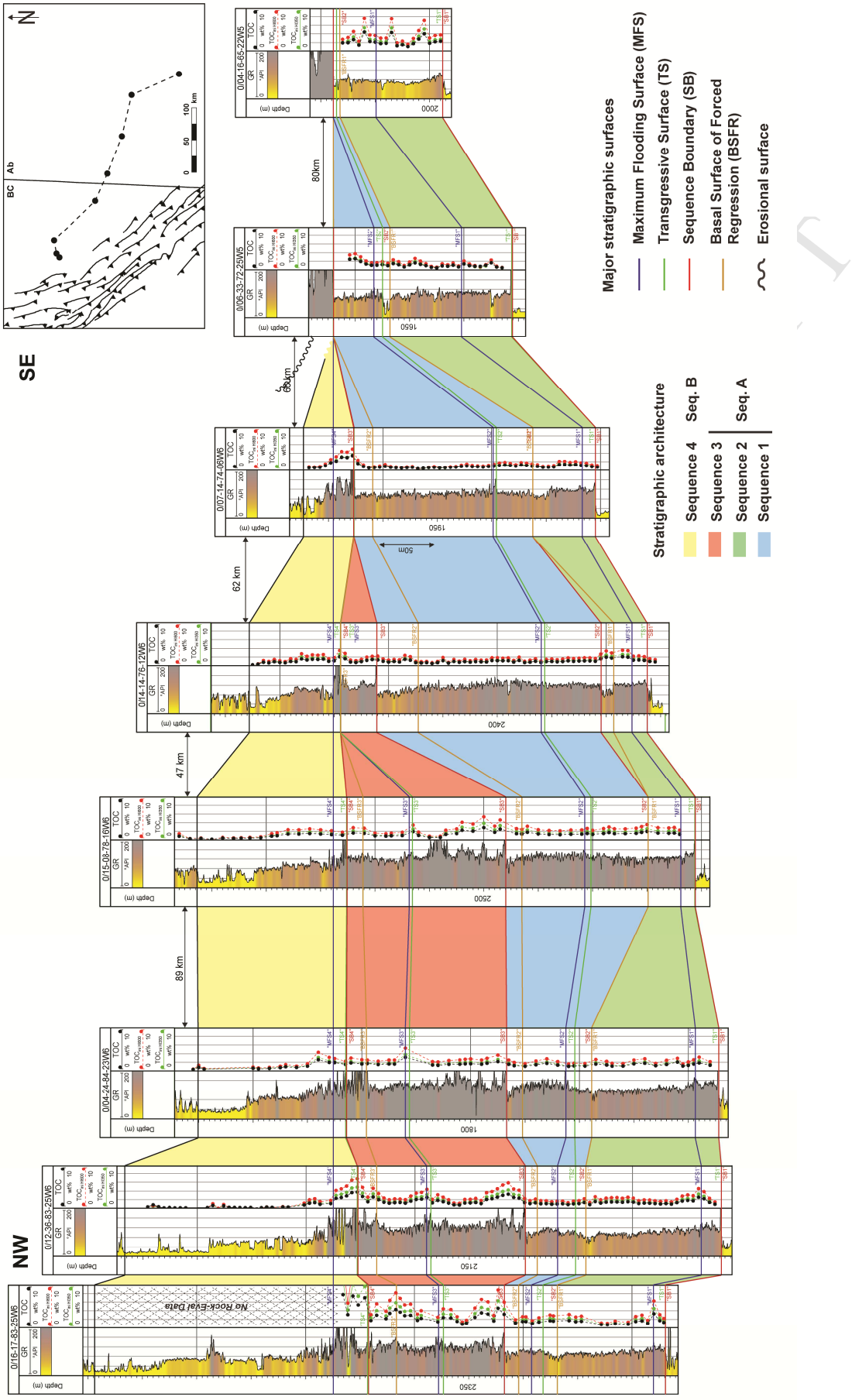

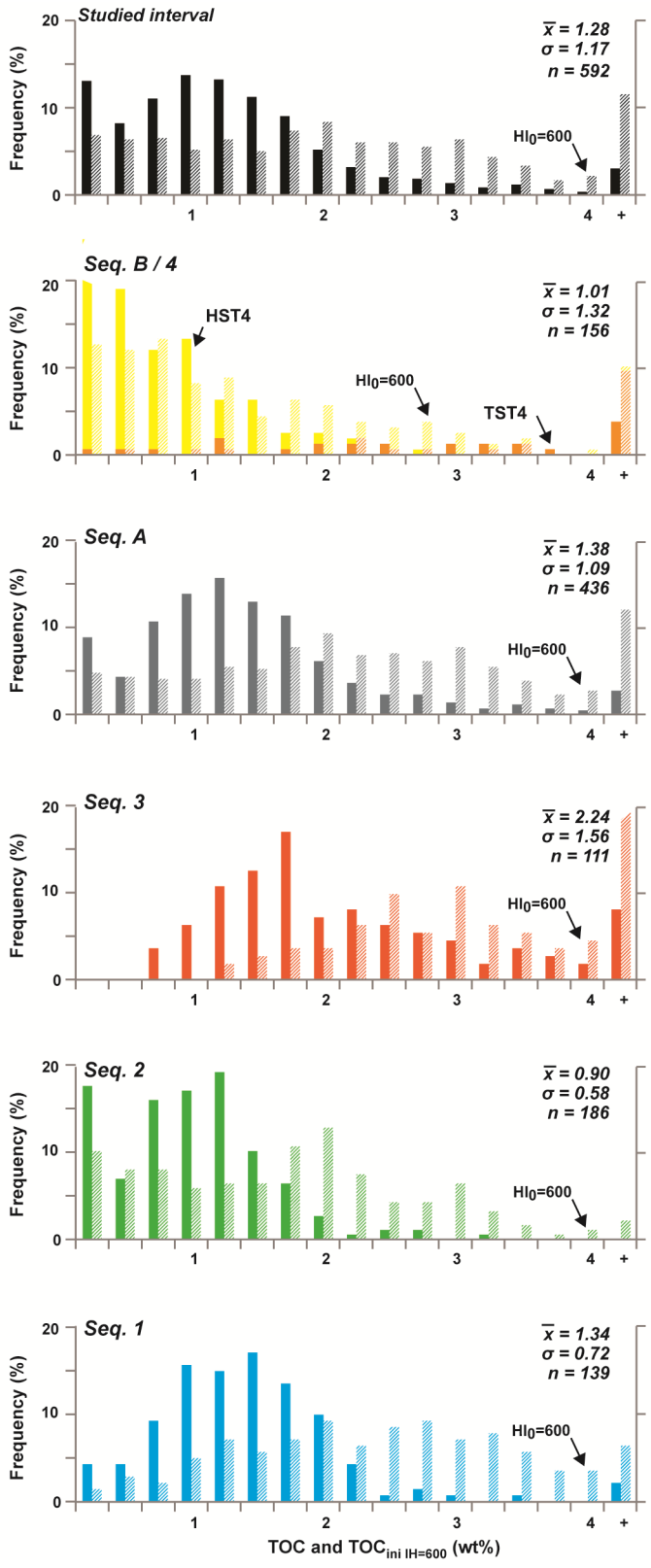

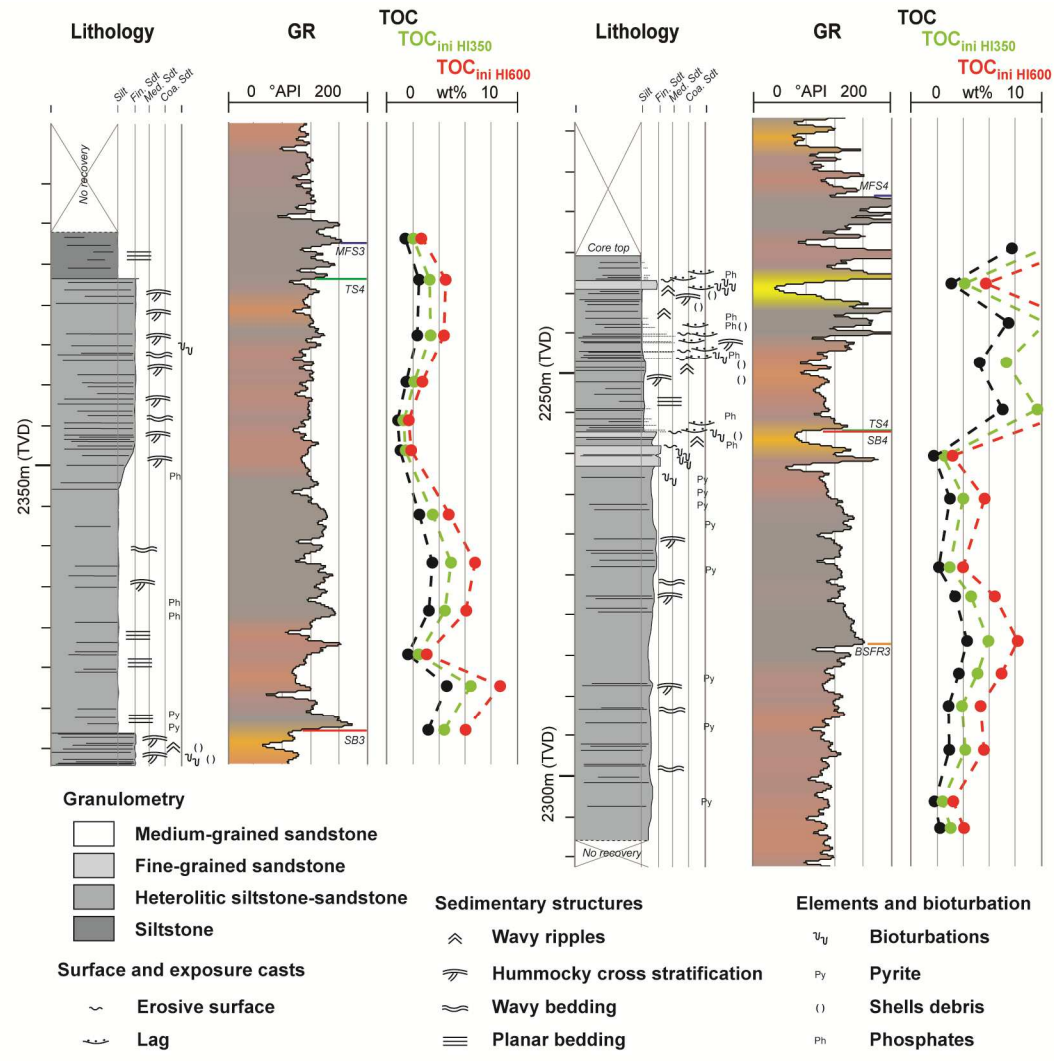
Lithology
GR
TOC
TOC ini HI350
TOC ini HI600
Silt
Fin. Sdt
Med. Sdt
Coa. Sdt
0 °API 200
0 wt% 10
No recovery
MFS3
TS4
SB3
2350m (TVD)
Core top
MFS4
SB4
BSFR3
2250m (TVD)
2300m (TVD)
Granulometry
Medium-grained sandstone
Fine-grained sandstone
Heterolitic siltstone-sandstone
Siltstone
Surface and exposure casts
Erosive surface
Lag
Sedimentary structures
Wavy ripples
Hummocky cross stratification
Wavy bedding
Planar bedding
Elements and bioturbation
Bioturbations
Pyrite
Shells debris
Phosphates